universität wien

MASTERARBEIT | MASTER'S THESIS

Titel | Title

DNA-methylation expression in Nothobranchius fuzeri

verfasst von | submitted by

Brian Manfred Schild B.Sc.

angestrebter akademischer Grad | in partial fulfilment of the requirements for the degree of

Master of Science (MSc)

Wien | Vienna, 2025

Studienkennzahl lt. Studienblatt | Degree programme code as it appears on the student record sheet:	UA 066 220
Studienrichtung lt. Studienblatt | Degree programme as it appears on the student record sheet:	Joint-Masterstudium Evolutionary Genomics and Systems Biology
Betreut von | Supervisor:	Univ.-Prof. Dipl.-Biol. Dr. Ulrich Technau

Table of Contents

I. Overview of figures

II. Overview of tables

III. List of abbreviations

Abbreviation	Description
β-Actin promotor	β-Actin promotor of ubiquitous and highly conserved structural protein
cDNA	Complementary DNA
Chr	Chromosome
sCMV promoter	Semian Cytomegalovirus immediate early enhancer and promoter
CO_2	Carbon dioxide
CRISPR/Cas9	Clustered regulatory interspaced short palindromic repeats/ CRISPR-associated protein
CRISPant	Individual edited by the CRISPR/Cas9 system
CS	Coding sequence
DAPI	4′,6-diamidino-2-phenylindole
DEPC	Diethyl pyrocarbonate
DMEM	Dulbecco's modified eagle medium
DNA	Desoxyribonucleic acid
dpf	Days post fertilization
dph	Days post hatching
E. coli	*Escherichia coli*
EDTA	Ethylenediaminetetraacetic acid
ef1α	Gene encoding for elongation factor 1-alpha
ef1α promotor	Elongation factor 1 alpha promoter
egfp	Gene encoding for enhanced green fluorescent protein (EGFP)
FBS	Fetal bovine serum
FELASA	Federation for Laboratory Animal Science Associations
FGF	Fibroblast growth factor
gfp	Gene encoding for green fluorescent protein
GRZ	*N. furzeri* strain from Gonarezhou national park MZM0403/10
HCl	hydrogen chloride
HEK293T	Human Embryonic Kidneys cells
HF	High fidelity
IVT	*In vitro* transcription
KO	knockout
LB medium	Luria Bertani medium
log2 FC	log2 fold change
M08	MZCS-08/122 strain of *N.furzeri*
Mb	Mega bases
MEM	Minimal Essential Medium
MOPS	3-(N-morpholino)propanesulfonic acid
mRNA	Messenger RNA
N. furzeri	*Nothobranchius furzeri*, turquoise Killifish
NaAc	Sodium acetate
PAM	Protospacer adjacent motif
PBS	Phosphate-buffered saline
PCR	Polymerase chain reaction
RNA	Ribonucleic acid
RT	Room temperature
RT-qPCR	Reverse transcriptase quantitative PCR
sffv promotor	Spleen Focus-Forming Virus Promotor
sgRNA	Single guide RNA
S.O.C.	Super Optimal Broth with glucose
SOE-PCR	Splicing by overlap extension PCR
TAE	Buffer solution with Tris base, acetic acid and EDTA
tg	Transgene
TGF-β	Transforming growth factor beta

Tol2	Tol2 transposase
WT	Wild type
wph	weeks post hatching
XX	Female, carrying two X chromosomes
XY	Male, carrying one X and one Y chromosome

IV. Zusammenfassung

Altern ist ein komplexer Prozess, der durch genetische, Umwelt- und epigenetische Faktoren geprägt wird, dabei spielen Modifikationen der DNA, wie die DNA-Methylierung eine zentrale Rolle bei der Regulation der Genexpression. Der sehr kurzlebige Killifisch (*Nothobranchius furzeri*) stellt ein einzigartiges Wirbeltiermodell dar, um epigenetische Dynamiken über die Lebensspanne im Kontext des Alterns zu untersuchen.

Ziel dieser Arbeit war es, die Rolle der Ten-Eleven-Translokation (Tet)-Enzyme und der DNA-Methyltransferasen (Dnmts) bei der Modulation der DNA-Methylierung und deren Einfluss auf Entwicklung und Alterung zu erforschen. Hierfür wurde eine *tet3*-Knockout-Linie im GRZ Hintergrund *in vivo* mittels CRISPR-Cas9 erzeugt. Trotz hoher embryonaler Mortalität, suboptimaler Eiqualität und Mosaizismus konnte *tet3* erfolgreich editiert und ein funktioneller Knockout erzielt werden. Dies demonstrierte das grundsätzliche grundsätzliche Potential eine stabile Knockout-Linie zu erzeugen.

Darüber hinaus wurde die Expressionsstärke der *dnmts* in Darm, Gehirn und Gonaden von männlichen und weiblichen Fischen in drei Lebensstadien untersucht. Dabei zeigte sich in den Gonaden eine ausgeprägte männliche Dominanz der *dnmt* Expression über alle Altersgruppen, im Darm trat diese nur bei alten Individuen auf, und dnmt1 war in alten Männchen deutlich hochreguliert, was eine geschlechtsspezifische Divergenz im späten Leben aufzeigen könnte. Die Expression im Gehirn war variabel und zeigte keine konsistenten Muster. *In-vitro*-Experimente demonstrierten eine erfolgreiche lentivirale Transduktion von tet1 in *N.furzeri* M08-abgeleiteten Fibroblasten und etablierten damit eine Plattform zur funktionellen Manipulation der *tet*-Aktivität.
Diese Ergebnisse liefern einen umfassenden Einblick in gewebespezifische, geschlechts- und altersabhängige *dnmt*-Dynamiken in *N. furzeri*, zeigen die Machbarkeit der *tet3*-Knockouterzeugung und etablieren Methoden zur gezielten Modulation der *tet*-Aktivität *in vitro.*

V. Abstract

Aging is a complex process shaped by genetic, environmental, and epigenetic factors, with DNA methylation serving as one of the epigenetic key regulators of gene expression. The short-lived turquoise killifish (*Nothobranchius furzeri*) offers a unique vertebrate aging model and best suited to study epigenetic dynamics across the lifespan. This thesis explored the roles of Ten-Eleven Translocation (TET) enzymes and DNA methyltransferases (DNMTs) in modulating DNA methylation and their impact on development and aging.

To this end, a *tet3* knockout line was generated in the short-lived *N. furzeri* GRZ strain the using CRISPR-Cas9 methodology. Despite challenges including high embryonic mortality, suboptimal egg quality, and mosaicism, successful editing and the generation of knockouts were achieved, demonstrating that stable line establishment is feasible with optimized protocols.

Moreover, *dnmt* expression was profiled across gut, brain, and gonads in males and females at three life stages. Gonads showed a strong male-biased expression across all ages, gut expression became male-biased only in old individuals, and DNMT1 exhibited pronounced upregulation in old males, indicating a late-life sex-specific divergence. Brain expression patterns were variable and lacked consistent trends. Complementary *in vitro* experiments demonstrated successful lentiviral transduction of TET1 in M08-derived fibroblasts, establishing a platform for functional manipulation of TET activity despite challenges from construct size and promoter silencing.

Together, these findings provide a comprehensive view of tissue-, sex-, and age-specific DNMT dynamics in *N. furzeri*, demonstrate the feasibility of *tet3* knockout generation, and establish a method for modulating TET activity *in vitro*.

1. Introduction

1.1 Epigenetic regulation and aging

Aging is characterized by a progressive decline in organismal functions and by hallmarks of molecular alterations, notably including epigenetic changes. These modifications occur at multiple regulatory levels, including chromatin remodeling, histone modifications, DNA methylation, and modification of RNA and non-coding RNAs. Among them, DNA methylation plays a central role by influencing chromatin structure and gene expression without altering the underlying DNA sequence. Together, these epigenetic mechanisms contribute to the aging process and to age-associated diseases by shaping transcriptional programs and cellular identity[1].

During aging, characteristic shifts in the methylome occur. Global hypomethylation, particularly affecting repetitive and intergenic regions, is accompanied by site-specific hypermethylation, often in promoter-associated CpG islands. These age-associated methylation changes have been observed across species, including humans and mice, and are proposed to contribute to genomic instability, disrupted gene regulation, and the development of age-related diseases [1,2].

The progression of DNA methylation changes correlates strongly with chronological age, giving rise to the development of so-called epigenetic clocks. Trained on methylation patterns at specific CpG sites, these clocks can accurately estimate biological age and have even been shown to predict life expectancy and age-related disease risk. This suggests that epigenetic drift may not merely reflect the passage of time but may also actively shape the aging trajectory [2,3].

Epigenetic modifications thus represent a dynamic layer of gene regulation that integrates environmental and cellular signals without changing the DNA sequence. In particular, the regulation of gene expression through DNA methylation and demethylation forms a central mechanism in both aging physiology and pathology. These processes underlie epigenetic aging markers and may play a direct role in the functional decline observed during aging [4].

1.2 Methylation and demethylation: biological roles and mechanisms

DNA methylation and active demethylation play essential roles in regulating gene expression, maintaining genomic integrity, and guiding developmental processes.

DNA methylation and its active reversal are essential for regulating gene expression, preserving genomic integrity, and guiding development. These modifications control chromatin accessibility, thereby modulating transcriptional activity at developmental genes, imprinted loci, and repetitive elements. Beyond development, they also influence cellular responses to environmental signals and stress. Dysregulation of methylation and demethylation has been linked to tumorigenesis [5–7], neurodevelopmental disorders [8,9], developmental abnormalities [6,10] and age-related functional decline [9,11,12]. The interplay between methylation and demethylation thus constitutes a critical axis of epigenetic regulation affecting health and disease susceptibility.

Cytosine methylation, primarily at CpG dinucleotides, is catalyzed by DNA methyltransferases (DNMT1, DNMT3A, DNMT3B). DNMT1 maintains existing methylation patterns during DNA replication, ensuring epigenetic inheritance, whereas DNMT3A and DNMT3B catalyze *de novo* methylation during development and differentiation [13,14].

Conversely, active DNA demethylation is mediated by the ten-eleven translocation (TET) family of dioxygenases (TET1, TET2, TET3), which successively oxidize 5-methylcytosine (5mC) to 5-hydroxymethylcytosine (5hmC), 5-formylcytosine (5fC), and 5-carboxylcytosine (5caC). These oxidized intermediates are then excised via thymine DNA glycosylase (TDG)-mediated base excision repair, enabling locus-specific demethylation [7].

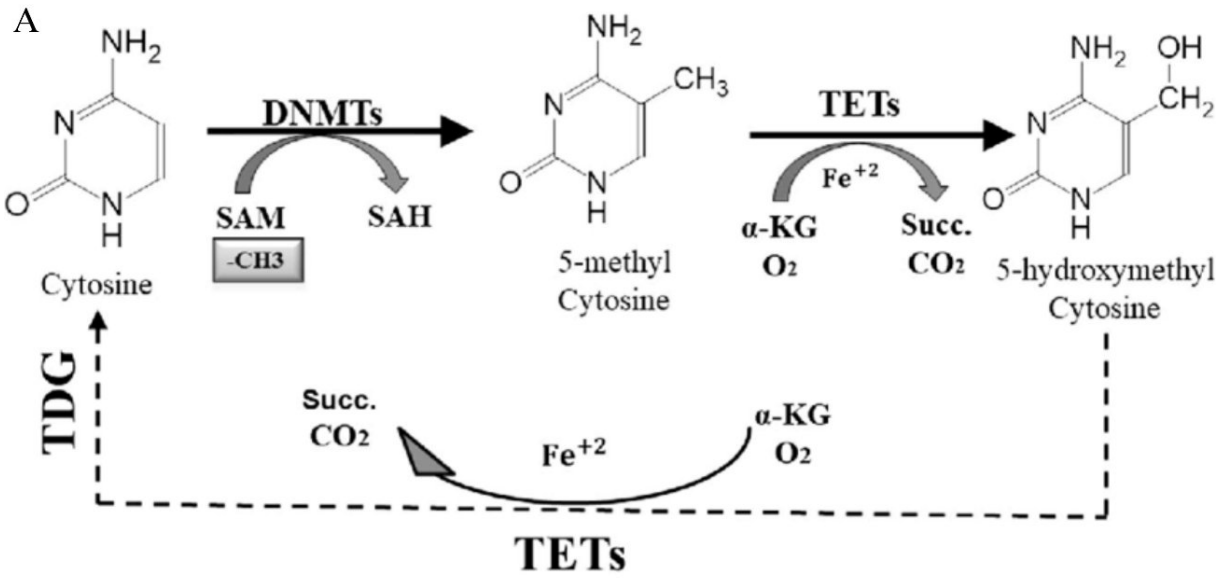

Figure 1 DNA methylation and demethylation process: DNA methylation occurs at the 5' position of cytosine, within CpG dinucleotides. DNMTs catalyze the transfer of the methyl group to cytosine and generate 5-mC using SAM as methyl donor and producing SAH. DNA demethylation is a multi-step oxidation process catalyzed by TETs methylcytosine dioxygenases family that uses Fe^{+2} and a - ketoglutarate as cofactors or substrates and generates succinate and CO_2. In the first step of demethylation process, the 5-mC is converted to 5-hmC, and after several oxidation reactions the methyl group can be remove by TDG-mediated base excision repair mechanism. (Figure adapted from Pop et al., 2019; [15] created with Biorender)

TET-dependent demethylation plays key roles in development, cellular differentiation, and responses to environmental stimuli [16–19]. Additionally, passive demethylation can occur through the dilution of methylation marks during DNA replication, particularly when DNMT1 activity is reduced [20]. Together, these reversible methylation dynamics form a finely tuned epigenetic system regulating transcriptional fidelity, genome stability, and physiological adaptability [4].

1.2.1 Evolution of TETS and DNMTs

DNA methyltransferases are widely conserved across life, deriving independently from prokaryotic methyltransferases and diversifying early in plant and animal evolution. Their copy numbers and even presence have shifted repeatedly across lineages [21]. In animals, TET enzymes emerged within the broader TET/JBP family, enabling active or replication-coupled demethylation [22]. Phylogenetic analyses suggest the TET/JBP family has deep roots, with members in bacteriophages, some bacteria, and diverse eukaryotes, followed by lineage-specific expansions and losses [23]. Across chordates specifically, whole-genome duplications expanded *tet* and *dnmt* repertoires, supporting specialization of maintenance versus *de novo* methylation and demethylation functions [24]. DNMT-mediated methylation and TET-mediated oxidation probably co-evolved as a dynamic regulatory system, with DNA methylation patterns themselves showing rapid evolutionary turnover, even complete loss, in multiple eukaryotic groups [25].

In *N. furzeri*, the DNA methyltransferase family includes one copy of Dnmt1, two copies of Dnmt3a (Dnmt3aa&ab), and one copy of Dnmt3b(a), all of which are homologues of their mammalian counterparts DNMT1, DNMT3A, and DNMT3B. The TET protein family consists of one copy of each paralogue. TET1, TET2, and TET3, analogous to the three *tet* genes found in humans, as shown in Figure 2.

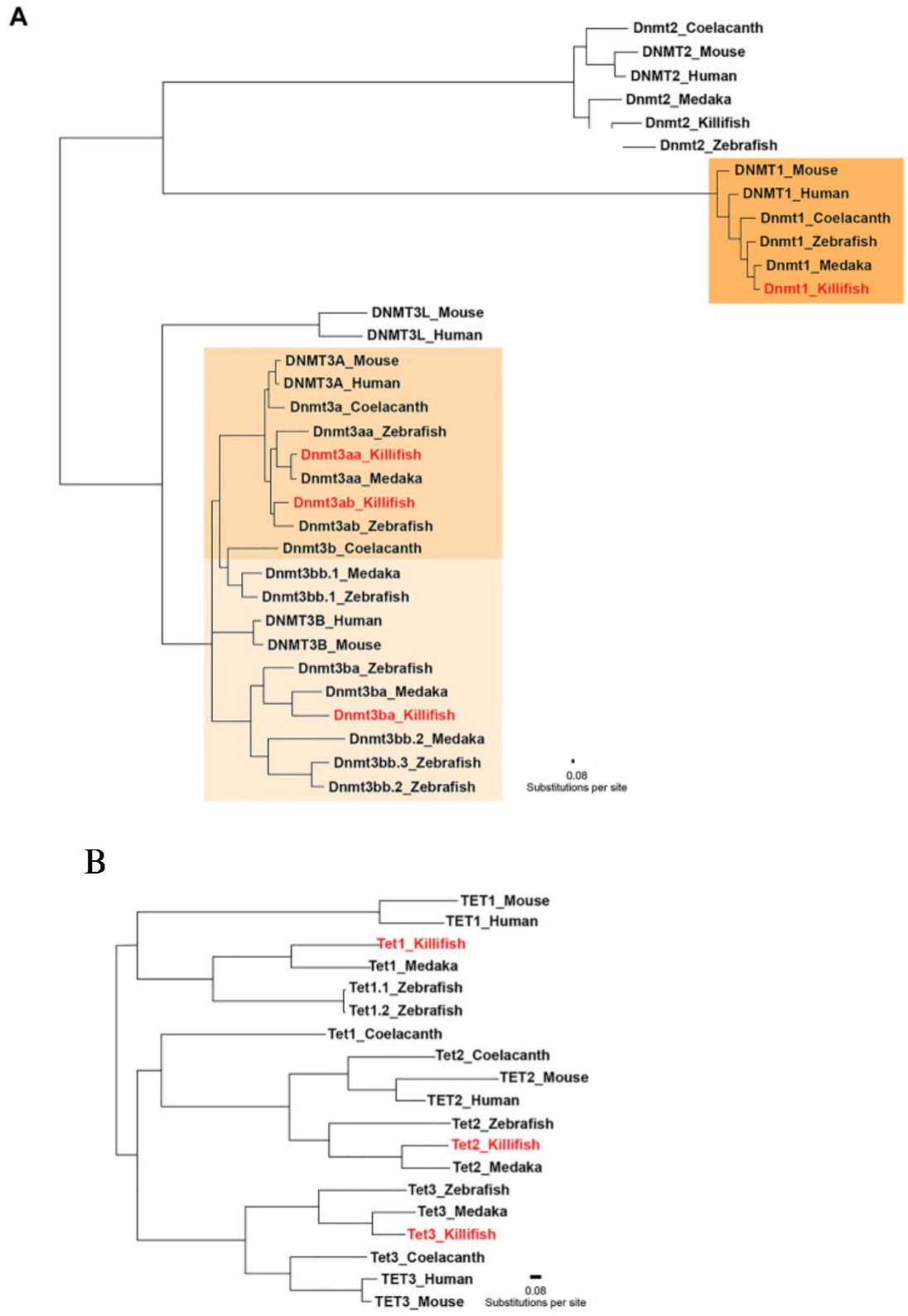

Figure 2 Phylogenetic relationships between key enzymes constituting the DNA methylation machinery. **(A)** Phylogenetic tree of vertebrate DNA methyltransferases (DNMTs) **(B)** DNMT1 and ten-eleven translocation methylcytosine dioxygenases (TETs) computed by the Maximum-Likelihood algorithm. Full protein sequences obtained from the following species were used: human (*Homo sapiens*), mouse (*Mus musculus*), zebrafish (*Danio rerio*), medaka (*Oryzias latipes*), killifish (*Nothobranchius furzeri*), and coelacanth (*Latimeria chalumnae*). Coelacanth represents a sarcopterygian fish illustrating the transition to a terrestrial life, creating modern tetrapods. The scale bar represents number of substitutions per site. (Figure adapted from Zupkovitz et al., 2021;[26] created with Biorender)

1.3 *Nothobranchius furzeri* as model organism in aging research

The turquoise killifish (*Nothobranchius furzeri*) has become a prominent vertebrate model for aging research, chiefly due to its remarkably short lifespan - typically three to six months under laboratory conditions (GRZ inbred line) - which is the shortest known among captive vertebrates [27–29]. Native to ephemeral freshwater pools in Mozambique and Zimbabwe, *N. furzeri* has evolved distinctive life history strategies shaped by the extreme transience of its habitat. These pools form briefly during seasonal rains and desiccate rapidly, imposing strong selective pressures that have favoured accelerated growth, early sexual maturity, and rapid reproduction [30].

A particularly striking adaptation to this unpredictable environment is embryonic diapause — a reversible developmental arrest allowing embryos deposited in the substrate to survive prolonged drought periods [28]. This process is supported by a specialized, resilient chorion that protects the embryos from dehydration, ensuring successful development once the rains return. These traits not only illustrate how ecological constraints can drive rapid life history evolution but also enable uniquely short experimental cycles, making *N. furzeri* exceptionally valuable for aging studies [31].

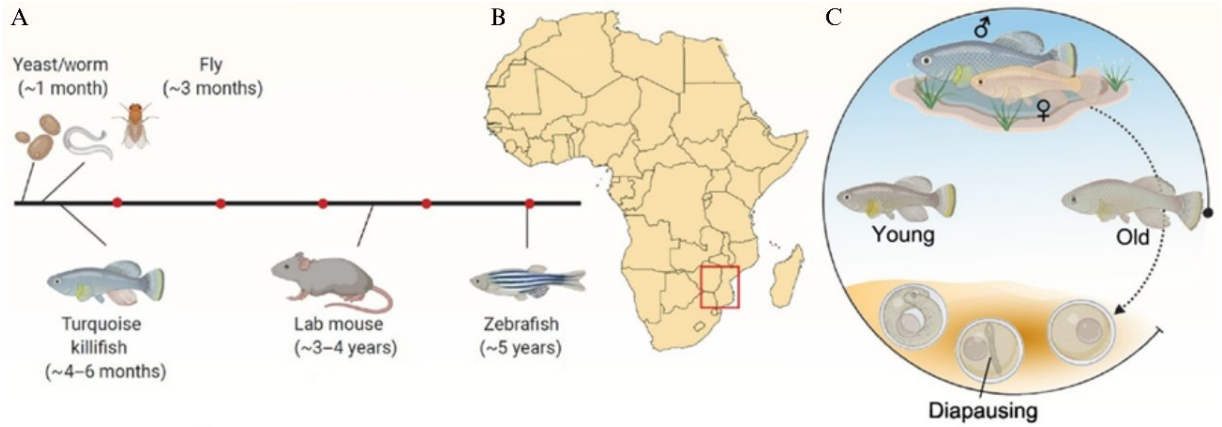

Figure 3 Lifecycle and occurrence of *Nothobranchius furzeri*. (A) Comparison of lifespan between model organisms. **(B)** Geographic origin of *N. furzeri*. **(C)** Simplified life cycle of *N. furzeri*. (Figure adapted from Zupkovitz et al., 2021; [32] created with Biorender)

Despite its short lifespan, *N. furzeri* displays hallmark aging phenotypes comparable to those observed in mammals, such as sarcopenia, cognitive decline, reduced tissue regeneration, and

accumulation of molecular damage, including increased DNA methylation drift and oxidative stress [27]. Importantly, dynamic changes in DNA methylation and hydroxy methylation patterns during aging have been documented, highlighting conserved roles for epigenetic regulators like DNMT and TET enzyme families [33–35].

Beyond its life history and phenotypic parallels with mammals, the turquoise killifish has benefited from significant methodological advances. The availability of a high-quality reference genome, comprehensive transcriptomic and methylomic datasets, and efficient gene-editing techniques such as CRISPR/Cas9 facilitate detailed functional analyses of aging-related genes [28,36]. Moreover, natural intraspecific variation in lifespan across wild-derived populations provides a unique opportunity to dissect how genetic background and environmental pressures shape longevity [37].

Altogether, the combination of a naturally compressed life cycle, vertebrate-conserved aging phenotypes, adaptability to environmental stress, and powerful genomic resources place *N. furzeri* as a versatile and time-efficient system for studying fundamental mechanisms of aging, epigenetic regulation, and the evolutionary interplay between environment and lifespan. [38] Its study not only advances understanding of fundamental mechanisms of aging and epigenetic regulation but also provides insights potentially translatable to longer-lived vertebrates, including humans.

1.4 Aim of this study

To elucidate the role of active DNA demethylation in vertebrate aging and development, a combined experimental strategy was implemented, integrating both *in vivo* and *in vitro* approaches targeting TET function. The principal aim is to dissect how modulation of TET enzymes affects DNA methylation landscapes, gene expression, and ultimately organismal phenotypes and developmental processes in the turquoise killifish (*Nothobranchius furzeri*).

In vivo, the establishment of a stable knockout line for *tet3* in the short-lived GRZ strain was planned by microinjection of a CRISPR/Cas9 system into fertilized one-cell stage embryos, following the protocol described by Harel et al.; 2015 [39]. This method enables targeted gene disruption at the earliest developmental stages, resulting in systemic loss-of-function throughout the organism. Previous work of H. Mörl (unpublished data) successfully applied a comparable CRISPR/Cas9-based strategy to generate knockouts of *tet* family genes in the

longer-lived M08 strain, thereby demonstrating both the technical feasibility and biological relevance of this approach in *N. furzeri*.

In parallel to the *in vivo* knockout, an in cell culture overexpression system for *tet1* was designed to investigate the consequences of elevated demethylation activity in killifish cells. Initial attempts using lipofection, a method widely employed in mammalian HEK cells, failed to achieve sufficient transfection efficiency in *N. furzeri* cells. To overcome this limitation, lentiviral transduction was used and showed good efficiency in preliminary tests with an EGFP reporter construct. Building on these findings, lentiviral vectors were subsequently used to overexpress *tet1* in killifish cell lines, enabling the examination of cellular proliferation, viability, and epigenetic remodelling under conditions of enhanced TET activity. Anticipated outcomes include phenotypic changes such as growth alterations, modified lifespan, or embryonic lethality in knockout fish, alongside changes in cell proliferation, differentiation, or methylation profiles in overexpression systems.

In addition, expression analyses of *DNA methyltransferases* (*dnmts*) at the mRNA level were conducted using RT-qPCR. This included quantifying transcript levels of *dnmt1*, *dnmt3aa*, *dnmt3ab* and *dnmt3ba* across different tissues, sexes, and age groups. Since comprehensive datasets on *tet* mRNA expression patterns had already been established before (H. Mörl, unpublished data), the current focus was placed on dnmt expression patterns to gain insights into baseline mRNA levels as well as potential interactions between the two enzyme families. Given that TET enzymes mediate demethylation while DNMTs catalyse methylation, it is reasonable to hypothesize the existence of inverse correlations or coordinated regulation between their expression patterns.

2. Material

1.1 Biological material

Table 1: Overview of used biological material.

Organism / cell line	Description	Origin
Nothobranchius furzeri GRZ eggs	*N. furzeri* wild type strain eggs	provided by the fish facility of Beutenbergstraße 11, 07745 Jena
Nothobranchius furzeri GRZ *(KO:tet1)*	Transgenic *N. furzeri* with tet knock-out	Generated in the framework of this thesis
Nothobranchius furzeri fin cells (strain: MZCS-08/122) *tg(sCMV:tet3)*	Transgenic *N. furzeri* fin cells, ectopically expressing sffv-driven *tet3*	Generated in the framework of this thesis
HEK273T tg(sffv:*tet3*)	Human Embryonic Kidney cells ectopically expressing sffv-driven *tet3*	
One Shot™ TOP04 *Escherichia coli*	Chemical competent *E. coli*	Invitrogen™ (Cat. Nr.: C404010)
One Shot™ TOP10 *Escherichia coli*	Chemical competent *E. coli*	Invitrogen™ (Cat. Nr.: C404003)

1.2 Devices

Table 2: Overview of used devices.

Device	Manufacturer
28°C CO_2CELL incubator (used for *N. furzeri* cells)	MMM Group
30°C Teco 20 Incubator (used for *N. furzeri* eggs)	Selutec
37°C Multitron Pro Incubator (used for bacteria)	INFORS HT
37°C CO_2 Incubator (used for HEK cells)	Panasonic
Agarose gel electrophoresis chamber	VWR International GmbH
Axio Zoom V16	Zeiss
Centrifuge 5424/ 5424 R	Eppendorf
CFX384TM Real-Time System	Bio-Rad
BD FACS Canto II (S1) analyse only	BD Bioscience
BD FACS Melody (S2) with cell sorting	BD Bioscience
Countess 3FL	Thermo Fischer
SteREO Discovery.V8	Zeiss
Electrophoresis power supply E83T	Consort BVBA
Eppendorf® Multichannel pipette	Eppendorf
Eppendorf® Multipette® plus	Eppendorf
Eppendorf® Research® plus pipette	Eppendorf
Eppendorf Xplorer electronic pipettor	Eppendorf
Flaming/ Brown micropipette puller (Needle puller P-97)	Sutter Instrument®
Gel DocTM XR	Bio-Rad
Injection plate	GT-Labortechnik
Injection plate stamp	GT-Labortechnik
VOYAGER electronic pipette	Integra
Mastercycler proS	Eppendorf
Molecular Imager® Gel DocTM XR+	BioRad
Nanodrop®	VWR International GmbH

Pressure injector – Pneumatic Pico Pump PV820	World Precision Instruments
SteREO Discovery.V8	Zeiss
Thermomixer compact	Eppendorf
TissueLyser II	QIAGEN
VOYAGER electronic pipette	Integra
Vortex 4 basic	IKA®

1.3 Consumables

Table 3: Overview of used consumables

Product	**Manufacturer**
Ceramic beads 1.4 mm	VWR International GmbH
6-Well plate	Thermo ScientificTM
12-Well plate	Thermo ScientificTM
24-Well plate	Thermo ScientificTM
96-Well plate	Thermo ScientificTM
384-well PCR plate	Bio-Rad
Falcon™ Tubes (15 ml, 50 ml)	Greiner Bio-One
Filter tips	StarLab
Borosilicate glass capillaries with filament GC100F-10 (1.0 OD x 0.58 ID x 100 L mm)	Havard Apparatus
384-well PCR plate	Bio-Rad
PCR stripes	Greiner Bio-One
Petri dish	Greiner Bio-One
Pipette tips 10µl, 20µl, 200µl, 1000µl	Sarstedt
Safe-Lock Tubes (1.5mL)	Eppendorf
Whatman Filters	GE Healthcare Life Sciences

1.4 Chemicals

Table 4: Overview of used chemicals.

Chemical	**Manufacturer**	**Catalogue number**
Acetic acid	Carl Roth	6755.1
Alpha FGF	ImmunoTools GmbH	11343555
Agarose tablets	Thermo Scientific™	R2801
Ammonium acetate	Carl Roth	631-61-8
β-Mercaptoethanol	Gibco™	31350010
Chloroform	Carl Roth	6340.1
SytoxBlue	Thermo Fischer	S34857
DAPI (4′,6-Diamidin-2-phenylindol)	Thermo Fischer	D1306
DEPC-treated H_2O	Carl Roth	T143.1
dNTPs	Thermo Scientific™	R0186
EDTA	Carl Roth	8043.2
Ethanol	Carl Roth	5054.1
Ethidium bromide solution 0.025 %	Carl Roth	HP47.2
FPS	Thermo Fischer	16000044
Formaldehyde	Merck	1.04003.1000
GlycolBlue	Thermo Fischer	AM9515
Isopropanol	Carl Roth	9866.1
MOPS	Carl Roth	6979.3
Penicillin/Streptomycin	Sigma-Aldrich®	34857

PFA	Merck	1.04005.1000
Phenolred	Merck	1.59375
ProLong™ Gold Antifade Mountant with DAPI	Invitrogen™	P36931
S.O.C. medium	Thermo Scientific™	15544.034
Sodium acetate	VWR International GmbH	27653.292
Sodium hydroxide	Merck	1.06498.1000
Sytox Blue	Thermo Fischer	
Tricaine methane sulfonate (MS-222)	Sigma-Aldrich	E19521
Tris	Carl Roth	5429.5
TRIzol® Reagent	ambion®	15596026

1.5 Buffers and solutions

Table 5: Overview of used buffers and solutions.

Buffer	**Composition**
0.3x Danieau's Buffer	17.0 mM NaCl 2 mM KCl 0.12 mM $MgSO_4$ 1.80 mM $Ca(NO_3)_2$ 1.50 mM HEPES pH 7.2
MOPS	83.6 g MOPS 33.2 ml 3 M NaAc 20 ml 0.5 M EDTA Fill up to 1 l with ddH_2O
2M NaAc (pH 4.0)	27.2 g sodium acetate 40 ml ddH_2O 35 ml acetic acid Adjust pH (4.0) with acetic acid
10x PBS (pH 7.4)	1.37 M NaCl 26.8 mM KCl 17.6 mM KH_2PO_4 101.4 mM Na_2HPO_4 in ddH_2O
4% PFA (pH 7.0)	20 g PFA 450 ml DEPC-treated H_2O 1.75 ml 2 M NaOH 50 ml 10X PBS Adjust pH (7.0) with 2 M HCl
2X RNA loading dye	3.25 µl 6X loading dye (Thermo Scientific) 3.75 µl formaldehyde solution (37%) 1 µl 20X MOPS buffer 2 µl ethidium bromide solution (250 µg/ml)
50x TAE	242 g 2 M Tris-base 57.1 ml 1 M acetic acid 100 ml 0.5 M EDTA
Tris-HCl (pH 8.0)	12.11 g 2 M Tris-base Solved in 100 ml ddH_2O Adjust pH (7.0) with 1 M HCl

1.6 Kits

Table 6: Overview of used kits.

Kit Name	Manufacturer	Catalogue Number
iScript cDNA Synthesis Kit	Bio-Rad	1708891
Lenti-X™ Concentrator	Takara	631231
LipofectamineTm 3000 Transfection Reagent	Thermo Fischer	L3000008
SYBR® GreenER™ Kit	Invitrogen™	11761-500
Nucleospin™ Gel and PCR Clean-up Kit	Macherey-Nagel™	11992242
QIAshredder	QIAGEN	79656
RNeasy Mini Kit	QIAGEN	74104
RNase-Free DNase Set	QIAGEN	79254
MAXIscript® T7 Transcription Kit	Invitrogen™	AM1314
Plasmid Maxi Kit	QIAGEN	12162

1.7 Enzymes and associated buffers

Table 7: Overview of used enzymes.

Enzyme	Manufacturer	Catalogue Number
DreamTaq DNA Polymerase (5 U/µL)	Thermo Scientific™	EP0701
T7 Endonuclease I	New England BioLabs	M0302L
Phusion™ High-Fidelity DNA Polymerase (2 U/µL)	Thermo Scientific™	F530L
NehI-HF	CutSmart^{Tm} Buffer	EheI
EcoRI-HF	CutSmart^{Tm} Buffer	Eam1105I

Table 8: Overview of used enzyme buffers.

Enzyme buffer	Manufacturer	Catalogue Number
DreamTaq™ Green Buffer (10X)	Thermo Scientific™	B71
NEBuffer 2	New England BioLabs	B7002S
Phusion HF Buffer	Thermo Scientific™	F518L

1.8 Plasmids

Table 9: Overview of used Plasmids

Plasmid	Origin	Function
300-pCS2-EGFP	Provided by Jochen Wittbrodt	Transfection plasmid with EGFP
psPAX2_#12260	Addgene	Lentiviral packaging vector; deposited by Didier Trono
pMD2.G_#12259	Addgene	Lentiviral envelope vector; deposited by Didier Trono
LeGo-iG2_#27341	Addgene	Lentiviral vector; deposited by Boris Fehse
tet1_attL_sites_in_pUC-GW	Genewiz from Azanta Life Sciences	plasmid with *tet1* insert for cloning
LeGo_tet1_EGFP_ssfv	Cloning product	Expression vector for cell

		transfections
LeGo_tet1_EGFP_sCMV	Cloning product	Expression vector for cell transfections

1.9 Ladders

Table 10: Overview of used DNA and RNA ladders.

Ladder	**Manufacturer**	**Catalogue Number**
GeneRuler™100 bp Plus DNA ladder	Thermo Scientific™	SM0321
GeneRuler™1 kp Plus DNA ladder	Thermo Scientific™	SM1331

1.10 Oligonucleotides

Table 11: Oligonucleotides used in SOE-PCR.

(Synthesized by Eurofins Genomics) Sequence orientation is 5' to 3'.

Primer	Sequence (5´- 3´)
*tet3*_sgRNA-F (HM_081)	GAAATTAATACGACTCACTATAGGATAGGGTCCAACTTATTG TGGTTTTAGAGCTAGAAATAG
*tet3*_sgRNA-R (HM_082)	GAAATTAATACGACTCACTATAGGGCCCCATGGAAGCTAAG TGAGTTTTAGAGCTAGAAATAG
tracer_rev primer (AR179)	AAAAGCACCGACTCGGTGCCACTTTTTCAAGTTGATAACGG ACTAGCCTTATTTTAACTTGCTATTTCTAGCTCTAAAAC
forward amplification primer (TF7)	GAAATTAATACGACTCAC
revers amplification primer (pDRrvs)	AAAAGCACCGACTCGGTGC

Table 12: Oligonucleotides used in Genotyping and "Sexing" PCRs.

(Synthesized by Eurofins Genomics) Sequence orientation is 5' to 3'.

Locus / purpose	Forward primer	Sequence	Reverse primer	Sequence	Product size
tet3 / genotyping	tet3_sg1/2_f (HM_83)	CATGTTACACCTT TCCCATCCT	tet3_sg1/2_r (HM_84)	TCCTGTAGTGA AGGTGGTGTT G	315 bp
tet1 / insertion	tet1 _f (HM_139)	GTGTCCCATAGCT AAATGGGTG	tet1_r (HM_140)	TGCCAATGAG CGTGGGATT	148 bp
egfp / insertion	CA138_tdTo mato-GFP (CA_138)	ATGGTGAGCAAG GGCGAG	CA139_GFP #395 (CA_139)	TGATATAGAC GTTGTGGCTG	460 bp
X/Y / sexing	fwd_XY (AR_117)	GCGGGCGTCACA CTCTCTC	rev_XY (AR_605)	AGCAGTGCAT TCAAAGCTAA TGTG	X:780 bp Y:536 bp

Table 13: Oligonucleotides used in qPCR.

Sequence orientation is 5' to 3'.

Target gene	Forward primer	Sequence	Reverse Primer	Sequence	Product size (on cDNA)
eef1a1l1	eef1a1l1 (HM_89)	GAAGGAAGCCG CCGAGATG	eef1a1l1 (HM_90)	CAATGATGGTCA CGTAGTACTTG	143 bp
rpl13a	RPL13a_ex4/5 (HM_87)	GGGTTCTGGGC TATGAGGTG	RPL13a_ex6 (HM_88)	TACTGCGTGTTTC CTGCCAA	131 bp
dnmt1	dnmt1-fwd04 (BS_40)	TGCCGGAGATT CGTAACGG	dnmt1-rev04 (BS_41)	AGAGCGCTCATG TCCTTGC	139 bp
dnmt3aa	dnmt3aa-fwd03 (BS_46)	GGGGACCATTT GACCTGGTT	dnmt3aa-rev03 (BS_47)	ACCGCCCAGTTC CCTCATAA	96 bp
dnmt3ab	dnmt3ab-fwd02 (BS_50)	TAAGGACCAAC ACTTCCCCG	dnmt3ab-rev02 (BS_51)	GGGAAAACCAAA CACCCTCTC	85 bp
dnmt3ba	dnmt3ba2-fwd04 (BS_68)	TCCACGATCCT CCCTTGATA	dnmt3ba2-rev04 (BS_69)	GCCTGCAGTCAT CCTCACTT	197 bp

1.11 Cell culture material

Table 14: Overview of used media, additives and further solutions.

Cell culture material	Manufacturer	Catalogue number
Accutase® solution	Sigma-Aldrich®	A6964
β-Mercaptoethanol	Gibco™	31350010
DMEM, high glucose	Gibco™	41965
Fetal Bovine Serum	Sigma-Aldrich®	F7524
MEM Non-essential Amino Acid Solution (100X)	Sigma-Aldrich®	M7145
Dulbecco′s Phosphate Buffered Saline	Sigma-Aldrich®	D8537
Penicillin-Streptomycin	Sigma-Aldrich®	P4333
Trypsin-EDTA solution	Sigma-Aldrich®	T4174
Zellshield	Biochrome	W 13-0050

1.12 Software and online tools

Table 15 Used Software

Software	Manufacturer/Provider
Addgene	Addgene
Benchling	Benchling
BioRender	BioRender
BLAST	NLM NCBI
ChatGPT, version GPT-5	OpenAI
CFX Manager 3.1	Bio-Rad
CHOPCHOP (version 3)	Labun et al., 2019
Excel	Microsoft
Eurofins	Eurofins Genomics
Geneious Prime	Geneious
GraphPad Prism 9	GraphPad Software
ICE v2 CRISPR analysis tool	Synthego
NanoDrop® 3.0.1	Nanodrop technologies
NEBuilder® Assembly Tool	New England Biolabs
NFINgb	Genome Analysis group at Fritz-Lipmann Institute, Jena
Phyre2.2.	Structural Bioinformatics Group at Imperial College London
Primer-BLAST	National Library of Medicine
TIDE/TIDER	TIDE
Reverse Complement	bioninformatics.org
SMART	EMBL
SnapGene Viewer	SnapGene/ GSL Biotech
Word	Microsoft
ZEN Software Blue Edition (2.6 lite)	Zeiss
Zotero	Corporation for Digital Scholarship

3. Methods

3.1 Cell Culture

3.1.1 Cultivation of HEK293T cells

HEK293T cells were maintained in T75 culture flasks at 37 °C with 5 % CO_2 in Dulbecco's Modified Eagle Medium (DMEM; high glucose, with pyruvate) supplemented with 10 % fetal bovine serum (FBS). To ensure continuous growth, cells were routinely passaged under sterile conditions. For passaging, the culture medium was first removed, and the cells were washed with 3 ml PBS. Subsequently, 2 ml of trypsin were added, and the cells were incubated for approximately 5 min until detachment was observed, facilitated by gently tapping the flask. Detached cells were resuspended in 10 ml fresh medium, and 0.5 or 1 ml (1:10 or 1:20 dilution) of the respective cell suspension was transferred back into the flask with fresh medium added to a final volume of 10 ml for further cultivation.

3.1.2 Cultivation of adult and *N. furzeri* larvae cells

Nothobranchius furzeri M08 (MZCS-08/122 strain) fin cells were cultured in T75 flasks at 32 °C with 5 % CO_2 in Dulbecco's Modified Eagle Medium (DMEM) supplemented as detailed in Table 16. For continued cultivation, cells were regularly passaged under sterile conditions. To do so, the culture medium was first removed, and the cells were gently washed with PBS, followed by incubation with 2 ml of Accutase for approximately 15 min to facilitate detachment. Detached cells were then resuspended in fresh medium as described in section 3.1.1.

Table 16: Composition of the cell culture medium for *N. furzeri* cells.

Material	**Volume**
DMEM, high glucose	450 ml
Heat inactivated FBS	50 ml
1 mM MEM	500 µl
50 mM β-Mercaptoethanol	1 ml
Alpha FGF (50 µg/ml)	100 µl
Penicillin/Streptomycin	2.5 ml
Zellshield antimycotics	2.5 ml

3.1.3 Transfection

Transient transfections were carried out using Lipofectamine™ 3000 (Thermo Fischer) as transfection reagent. Approximately 50,000 cells were seeded per well in 24-well plates containing 1 ml of culture medium and transfected either immediately after seeding or after a 24 h pre-incubation period. For each transfection, two separate tubes were prepared following the protocol. The contents were then combined and incubated at room temperature for min15 min to allow complex formation. Afterwards, 50 µl of the transfection mixture were carefully added to each well. To assess transfection efficiency and cell viability, cells were counted using the Countess Automated Cell Counter (Thermo Fisher Scientific) with trypan blue exclusion for viability and EGFP fluorescence detection for identification of transfected cells. The transfection mix and procedure were carried out according to the manufacturer's protocol.

3.1.4 Transduction via Lentivirus

3.1.4.1 Preparation of Lentiviral Vectors

For the overexpression via lentiviral transduction, three vectors LeGO-iG2, pMD2.G and psPax2 from Addgene (https://www.addgene.org/) were used as components to assemble the complete lentivirus within a host culture of HEK293T cells. Initially, plasmids were isolated from transformed *E. coli* cells as described in the plasmid preparation section 3.2.4. Subsequently, the *tet1* coding sequence, ordered from GENEWIZ (https://www.genewiz.com/public/services/plasmid-dna-prep) in a plasmid, was cloned into the LeGO-iG2 backbone vector. Correct insertion was confirmed by Sanger sequencing (Eurofins). The cloning process followed the protocol detailed in 3.2.13 Molecular Cloning. The reaction setups for restriction digest and ligation are summarized in Table 17.

Table 17 Restriction Digest for *tet1* and LeGO Plasmids (left) and Ligation of *tet1* and LeGO (right)

Volume	Material
250 ng	LeGO-iG2 / GENEWIZ_tet1
2 µl	CutSmart buffer
1 µl	EcoRI-HF
1 µl	NotI
~15 µl	DEPC-treated H_2O
20 µl	total

Volume	Material
2 µl	T4 DNA ligase
2 µl	10x T4 ligase buffer
100 ng	LeGO-iG2
500 ng	tet1_attL_sites_in_pUC-GW
8,8 µl	DEPC-treated H_2O
20 µl	total

The final pLeGO backbone plasmid was designed to carry the *tet1* coding sequence, followed by an internal ribosome entry site (IRES) enabling bicistronic expression of the *egfp* reporter gene. In addition, an HA epitope tag was incorporated to facilitate subsequent detection and quantification of TET1 at the protein level.

*small epitope tag from influenza hemagglutinin used for antibody-based detection

Figure 4 Schematic representation of cloned pLeGO construct used for genomic integration and *in vitro* over-expression of *tet1*.

3.1.4.2 Lentivirus Transfection of HEK293T cells

For lentiviral production, HEK293T cells were seeded at a density of 2.5×10^6 cells in 10 ml of medium per T75 flask (or proportionally adjusted for T175 flasks) one day before transfection. Cells were incubated at 37 °C. On the second day, cells were transfected under S2 laboratory conditions. The transfection mix included the transfer vector pLeGO carrying *tet1*, the packaging plasmid PsPAX2, the envelope plasmid pMD2.G, and the corresponding transfection reagents as detailed in Table 19. The standard transfection protocol described in section 3.1.3 was followed. The transfection mix (see Table 19) was then added to the wells or flasks, depending on the experimental setup. Cells were incubated overnight at 37 °C.

Table 19 Transfection mix S2 (Quantities refer to the transfection of 10ml medium in a T75 flask).

Tube	Volume	Material
1	29,6 µl	Lipofectamine™ 3000
	750 µl	Opti-MEM
	40 µl	P3000
2	10 µg	LeGO-iG2
	5 µl	PsPAX2
	5 µl	pMD2.G
	750 µl	Opti-MEM

The next day, a medium change was performed. The cells were washed three times with PBS (each time using about half of the culture volume) before fresh medium was added. Viral supernatant was collected on days three and four post-transfection and centrifuged at 500 × g

for 10 min at room temperature to remove cellular debris. The clarified supernatant was subsequently mixed with one-third of its volume of Lenti-X™ Concentrator and incubated at 4 °C for at least 16 h. On day five, the mixture was centrifuged at 1,500 × g for 45 min at 4 °C. After carefully discarding the supernatant, the viral pellet was resuspended in 200 µl of VirusSaveTube™ solution. The concentrated viral preparations were then aliquoted and stored at −80 °C for later use in transduction experiments.

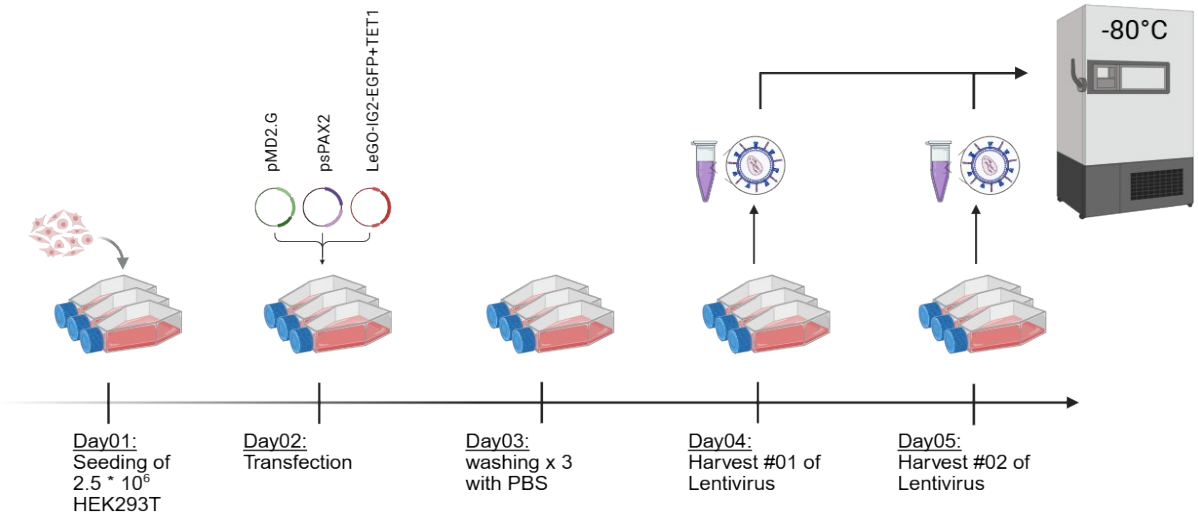

Figure 5 Schematic overview of the five-day workflow for lentivirus production

3.1.4.3 Lentiviral Transduction of N. furzeri fin cells

For transduction experiments, both HEK293T cells and *N. furzeri* fin-derived FiM cells were seeded at a density of $2.5x10^5$ cells per well/ml in 6-well plates. The following day, cells were treated with fresh culture medium supplemented with Polybrene (0.88µl polybrene/ml medium) to enhance viral entry. Lentiviral stocks, previously produced and concentrated as described, were thawed on ice and pooled. Serial dilutions of the virus were prepared to achieve a range of viral particle concentrations. Aliquots of these dilutions were added directly to the wells. Plates were gently swirled to ensure even distribution and incubated overnight at 37 °C.

Cells were washed three times with PBS (using approximately 50 % of the medium volume) to remove residual virus particles and Polybrene, and were then supplied with fresh, additive-free medium. On the next day, the culture medium was carefully renewed to maintain optimal

conditions for cell recovery and proliferation. On day five, cells were gently detached, transferred into fresh tubes, and centrifuged at 500 g for 10 min. After discarding the supernatant, the resulting cell pellets were resuspended in 300 µl PBS containing 10 % FBS. The suspension was filtered into 5 ml sample tubes equipped with integrated 35 µm filter caps to ensure a homogeneous single-cell preparation suitable for flow cytometry. Immediately prior to analysis, 0.3 µl of 1 mM Sytox™ Blue viability dye was added to enable discrimination of living and dead cells during FACS measurement.

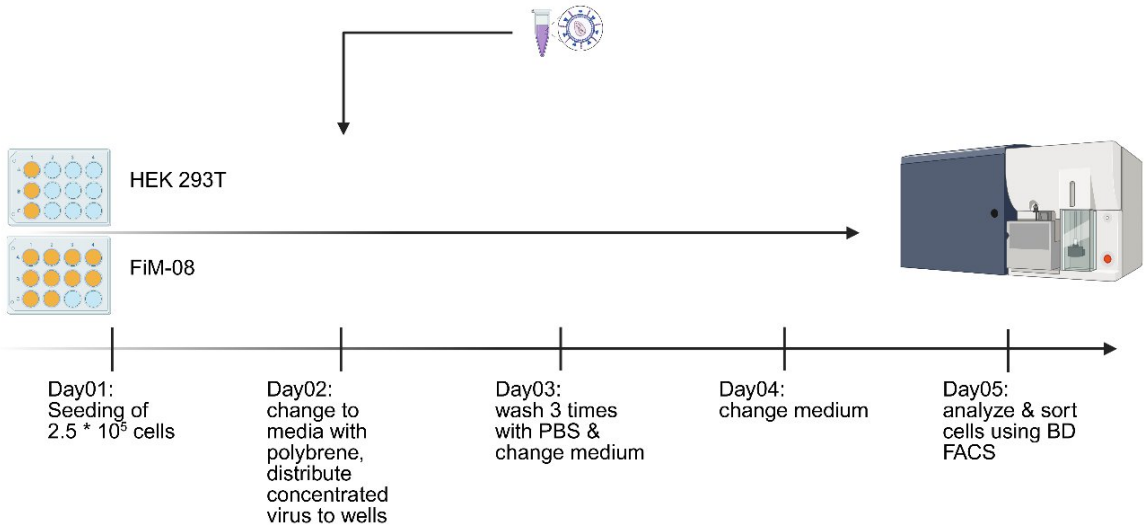

Figure 6 Schematic overview of the five-day workflow for transduction via Lentivirus

3.1.4.4 Analyses

To quantify transduction efficiency and selective enrichment of successfully transduced cell populations, fluorescence-activated cell sorting (FACS) was carried out in collaboration with the FACS facility staff. The gating strategy was tailored to the respective downstream application: initially, gates were defined based on cell size and the inclusion of live cells identified by Sytox Blue staining. To reduce background noise, the fluorescence threshold was set relative to the non-transfected control, ensuring that only genuinely transduced cells were detected.

In subsequent sorting experiments, the gating strategy was deliberately adjusted to include only cells exhibiting strong fluorescence signals. This more stringent gating was applied to minimize the risk of false-positive cells being sorted. The rationale behind this adaptation was the concern that even a small number of non-transduced and therefore potentially less stressed cells could

gain a growth advantage and rapidly outcompete the desired transduced population over the course of several days.

3.2 Molecular biological techniques

3.2.1 CRISPR-Cas9-mediated knockout

CRISPR-Cas9 genome editing introduces targeted double-strand breaks in DNA, which are repaired by the error-prone non-homologous end joining (NHEJ) pathway, often resulting in frameshift mutations and gene disruption. Cas9 mRNA was synthesized *in vitro*, and the injection mix, comprising sgRNA and Cas9 mRNA, was prepared under *RNase*-free conditions. Two sgRNAs targeting exon 4 of *tet3* according to the most recent genome assembly (NfurGRZ-RIMD1; GeneID: 107393527) were designed by H. Mörl to induce a frameshift mutation. Exon numbering corresponds to *tet1* transcript XM_070546394.1 as annotated in NCBI. For repeated injections, fresh batches of the same sgRNAs were produced.

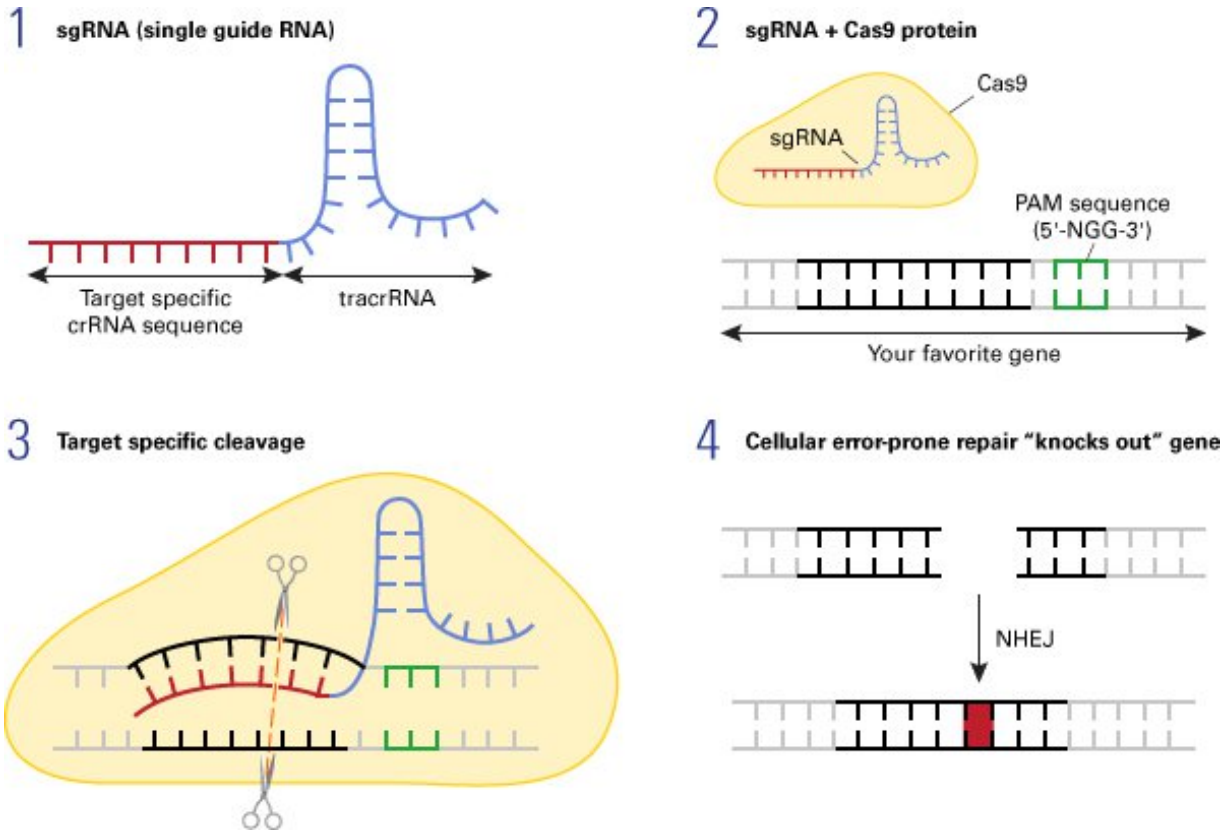

Figure 7 The principle of CRISPR/Cas9-mediated gene editing. A single guide RNA (sgRNA), consisting of a crRNA sequence that is specific to the DNA target, and a tracrRNA sequence that interacts with the Cas9 protein **(1)**, binds to a Cas9 DNA endonuclease **(2)**. The resulting ribonucleic protein complex will cause target-specific double-stranded DNA cleavage **(3)**. The cleavage site will be repaired by the nonhomologous end joining (NHEJ) DNA repair pathway, an error-prone process that may result in insertions/deletions (INDELs) that might disrupt gene function **(4)**. (Figure from Barrangou et al., 2015 [40])

3.2.2 Polymerase chain reaction

3.2.2.1 Sex determination

For sex determination a PCR (Table 20) with a primer pair hybridizing to chromosome 5 targeting *gdf6Y* has been used [41]. Depending on the sex of the respective individual, different sizes of PCR products were generated. In females, a PCR product of 706 bp length is formed as shown as in Figure 8, while in males an additional PCR product of 465 bp is expected. 10µl of PCR product was used for gel electrophoreses.

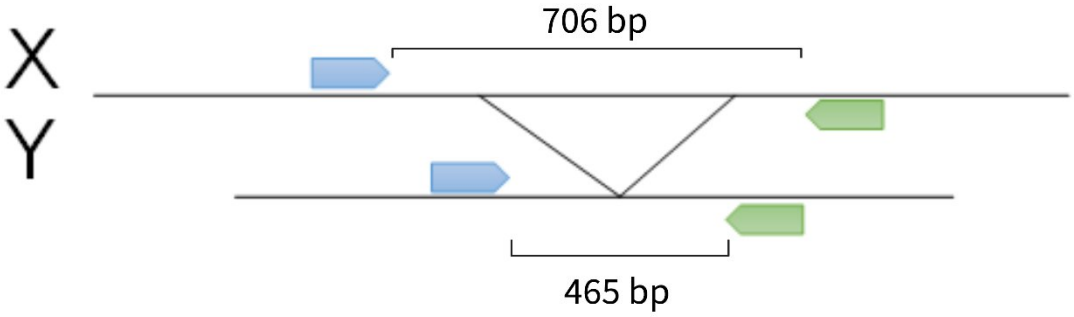

Figure 8 Schematic representation of the molecular sex determination assay. Due to a deletion in the DNA sequence on the Y chromosome, the same primer pair (blue/green arrows) lead to amplification of two different fragments from the sex chromosomes. This particular primer pair enables the detection of both sex chromosomes and thereby the discrimination of females (XX) and males (XY) in the short-lived, yellow-tailed inbred strain GRZ from Zimbabwe. (Figure adapted from Richter et al., 2022; [41] created with Biorender)

Table 20 Sexing PCR mix (left) and amplification program (right)

Volume	Material
2 µl	lysate
2 µl	Green Buffer
0.4 µl	10 mM dNTPs
0.4 µl	Primer fwd_XY
0.4 µl	Primer rev_XY
0.1 µl	Dream Taq polymerase
14.7 µl	DEPC-treated H_2O

Temperature	Time	Cycles
95 °C	5 min	
95 °C	30 sec	35
60 °C	30 sec	
72 °C	60 sec	
72 °C	5 min	
4 °C	hold	

3.2.2.2 Genotyping PCR

To assess whether embryos carried CRISPR/Cas9-mediated mutations in *tet3*, PCR amplification was performed using primers flanking the sgRNA target sites (see Table 21). In wild-type embryos, this reaction yields a single product of 505 bp (exon 4, Figure 9). Successful editing of the locus by sgRNA guided Cas9, using both sgRNAs, followed by error-prone non-homologous DNA repair (NHEJ) can introduce insertions or deletions (indels), resulting in additional products of variable size. In particular, a distinct band of 315 bp is expected if both sgRNAs induce a deletion spanning their target sites. For this analysis, locus-specific primers were used to amplify the region encompassing the predicted cut sites.

Table 21: *tet3* CRISPants genotyping PCR mix (left) and amplification program (right)

Volume	Material
3 µl	lysate
5 µl	Green Buffer
1 µl	10 mM dNTPs
1 µl	tet3_sg1/2_f
1 µl	tet3_sg1/2_r
0.25 µl	Dream Taq polymerase
38.75 µl	DEPC-treated H_2O

Temperature	Time	Cycles
95 °C	5 min	
95 °C	30 sec	35
51 °C	30 sec	
72 °C	35 sec	
72 °C	5 min	
4 °C	hold	

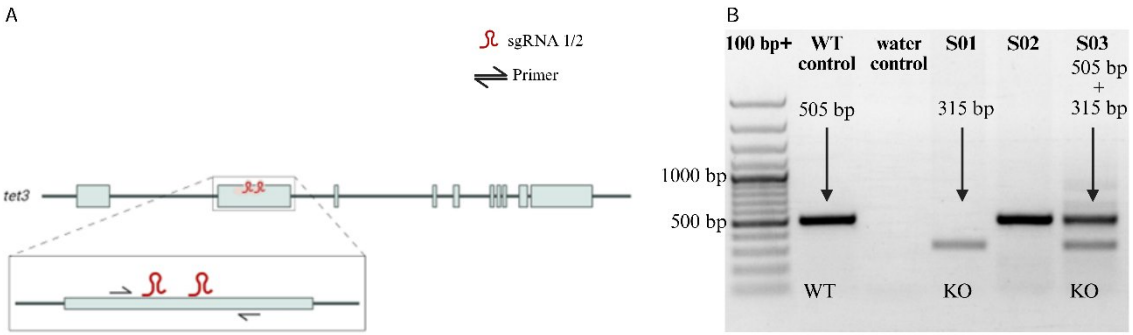

Figure 9 Overview of the genotyping PCR used for analyzing of Cas9 mediated editing of *tet3* **(A)** Schematic representation of sgRNA targeting exon 4 of *tet3* and primer binding sites used for diagnostic genotyping PCR. **(B)** Expected fragment sizes for wild-type (WT), samples (S01-03) and knockout (KO) alleles.

3.2.2.3 T7 endonuclease I assay

To identify small indels in CRISPR/Cas9-edited *tet3* embryos that were not detectable by standard genotyping PCR, a T7 endonuclease I (T7EI) assay was performed. For each reaction, 200 ng of purified PCR products were combined with 1 µl of NEB Buffer 2 (New England Biolabs) and brought to a final volume of 9.5 µl with DEPC-treated water. Samples were denatured and re-annealed in a thermocycler. Initial denaturation at 95 °C for 5 min, followed by cooling at −2 °C/s until 85 °C (held for 1 second), and then a slow cooling phase at −0.1 °C/s until reaching 25 °C. After re-annealing, 0.5 µl T7 Endonuclease I (≈ 5 units) was added, and the reaction was incubated at 37 °C for 15 min. The reactions were then placed on ice, and 2 µl of 6× loading dye containing EDTA were added to stop the enzyme activity. The complete reaction volume (~10 µl) was loaded onto a 1.5 % agarose TAE-gel for 45min at 110 V.

In wild-type embryos, the assay yields a single uncut PCR fragment of 515 bp. In contrast, if one or both sgRNAs successfully introduced mutations at the target site, T7EI recognizes and cleaves mismatched heteroduplexes formed during re-annealing, resulting in smaller restriction fragments that can be detected on the gel. The observed fragment pattern allows inference of which sgRNA was active and confirms CRISPR-mediated editing events.

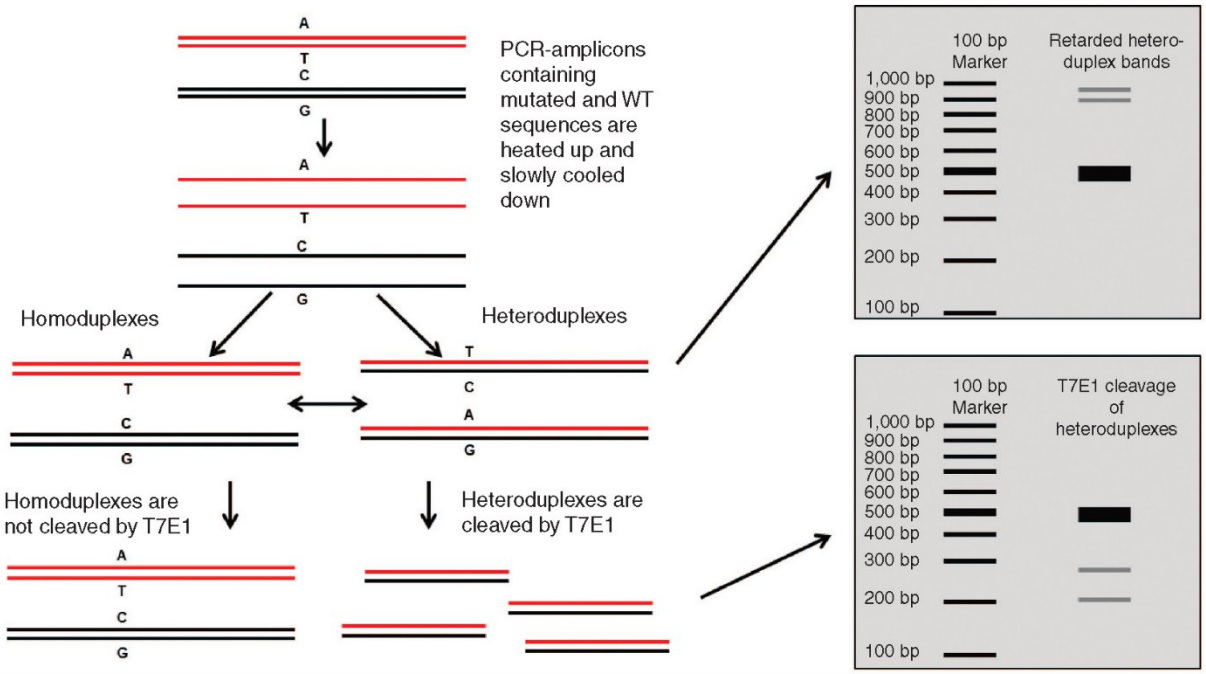

Figure 10 Schematic representation of the T7EI heteroduplex formation-based assay. The genomic locus surrounding the expected mutation site is PCR-amplified, denatured by heating, and reannealed by gradual cooling to form both homoduplexes and heteroduplexes. Mutated and unmutated PCR products can then be distinguished either by the presence of retarded bands on electrophoresis gels or by specific cleavage products generated through T7 endonuclease I (T7E1) digestion. (Figure adapted from Ehrke-Schulz et al., 2016; [42]created with Biorender)

3.2.3 DNA extraction & clean up from *N.furzeri*

For DNA extraction, eggs, black-eyed stage embryos, or cultured cells were incubated at 95 °C for 45 min in 50 mM NaOH (pH 12.7) Afterwards, 10 µl of Tris-HCl buffer (pH 8.0) were added to neutralize the solution. The resulting lysates were used for subsequent PCR.

PCR product purification was performed using the NucleoSpin™ Gel and PCR Clean-up kit (Macherey-Nagel). Typically, 50 µl of PCR products were processed following the manufacturer's protocol. For elution, 15–30 µl of *RNase*-free water were used in place of the supplied elution buffer. The DNA concentration of the purified samples was subsequently determined using NanoDrop.

3.2.4 DNA gel electrophoresis

To prepare an agarose gel, the appropriate quantity of agarose was dissolved in 1× TAE buffer to achieve the desired concentration and then melted completely by heating in a microwave oven. Once the solution had cooled to around 50 °C, ethidium bromide was added at a ratio of three drops per 100 ml. The molten agarose was subsequently poured at room temperature into a casting tray equipped with a comb and allowed to solidify.

The solidified gels were placed in an electrophoresis tank filled with 1× TAE buffer. PCR products (5 - 50 µl) were then carefully loaded into the wells formed by the comb. Electrophoresis was carried out at a voltage of 110–140 V for approximately 30 -60 min, depending on the sample volume and the requirements of downstream analysis. Finally, the gels were visualized and recorded using the Molecular Imager® Gel Doc™ XR+ system in combination with Image Lab™ software.

3.2.5 Preparation of plasmid DNA by maxi prep

For large-scale plasmid preparation, individual transformed *E. coli* colonies were inoculated into 200 ml of LB medium containing the appropriate antibiotic (1:1000 dilution) and incubated overnight at 37 °C with shaking. The bacterial cultures were harvested by centrifugation, and plasmid DNA was purified using the QIAGEN Plasmid Maxi Kit following the manufacturer's instructions. The concentration and purity of the isolated plasmid DNA were subsequently assessed with a NanoDrop spectrophotometer.

Samples from successful Maxi Prep were submitted for Sanger sequencing for verification.

3.2.6 RNA isolation from *N. furzeri* tissue

Total RNA was isolated from *N. furzeri* tissue using the RNeasy Mini Kit according to the manufacturer's instructions, with on-column *DNase* digestion to remove genomic DNA contamination. Briefly, tissues were homogenized in RLT buffer supplemented with β-mercaptoethanol using ceramic beads and a TissueLyser (30 Hz, 2 min). To isolate the RNA was centrifuged and mixed with 70 % ethanol, loaded onto RNeasy spin columns, and subjected to sequential washes with RW1 and RPE buffers. *DNase* I treatment (prepared freshly by mixing *DNase* with RDD buffer) was performed directly on the column and followed by additional wash steps. RNA was eluted in 30–50 µl *RNase*-free water, and concentration and purity were assessed using a NanoDrop spectrophotometer. Samples were stored at -80°C.

3.2.7 sgRNA Synthesis

Single-guide RNAs (sgRNAs) were synthesized *in vitro* by T7 RNA polymerase. For this, templates were generated by single overlap extension PCR (SOE-PCR) using Phusion polymerase and gene-specific primers, designed by H.Mörl. The forward primer (tet3_sgRNA-F/R) contained a T7 promoter, the guide sequence, and part of the tracr sequence, while the reverse primer (tracer_rev primer) completed the tracr sequence due to its specific overhangs. The resulting product was further amplified with TF7 and pDRrvs primers (Table 11, Figure 11). PCR reactions were carried out according to the program listed in Table 22.

Table 22 SOE PCR mix (left) and amplification program (right)

Volume	Material
1 µl	sgRNA-F/R primer primer 0.1µM
1 µl	tracer_rev primer 0.1µM
1 µl	dNTPs 10 µM
10 µl	HF Buffer
2,5 µl	TF7 primer 10 µM
2,5 µl	pDRrvs primer 10 µM
0,5 µl	Phusion polymerase
1,5 µl	DEPC-treated H_2O

Temperature	Time	Cycles
98 °C	30 sec	
98 °C	10 sec	x 40
50 °C	20 sec	
72 °C	10 sec	
72 °C	5 min	
4 °C	hold	

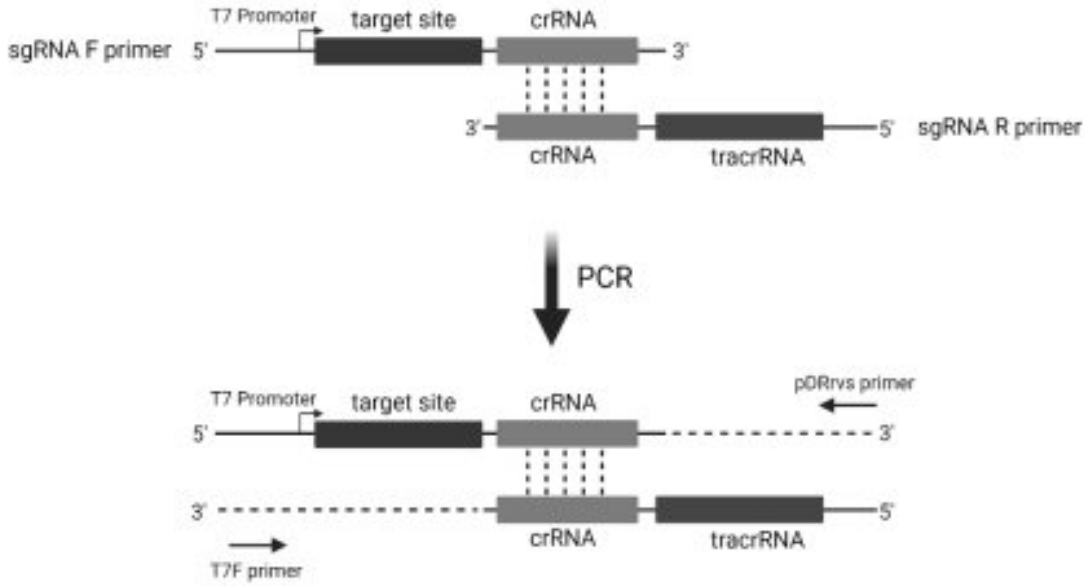

Figure 11 SOE PCR to generate a template for the *in vitro* synthesis of sgRNAs. The sgRNA F primer contains a T7 promoter for subsequent *in vitro* transcription (IVT), the specific target site and a crRNA sequence. The crRNA sequence allows the sgRNA F and R primer to hybridize in this region. In a polymerase chain reaction, the overhangs are filled up and the template is generated. The AR183 and AR072 primer can now bind to the template and a PCR-based amplification can take place. (adapted from Markus Kleemann, unpublished)

Amplified PCR products (~100 bp) were verified on a 2 % agarose gel, pooled, and purified using Macherey Nagel NucleoSpin™ Gel and PCR Clean-up kit, eluted in 15 µl DEPC-H_2O and concentration was assessed via NanoDrop.

For *in vitro* transcription (IVT), ~1 µg of purified template was incubated overnight at 37 °C using the MAXIscript® T7 Transcription Kit (Table 23).

Table 23 *In vitro* transcription mix

Volume	Material
1µg	SOE-PCR product
1 µl	UTP
1 µl	ATP
1 µl	GTP
1 µl	CTP
2 µl	T7 enzyme mix
2 µl	10x T7 reaction buffer
~ 10 µl	DEPC-treated H_2O

On the following day, residual template DNA was removed by *DNase* digestion with 1µl TURBO *DNase* (15min, 37°C), and the sgRNAs were precipitated using ammonium acetate and ethanol in the presence of GlycoBlue to aid visualization. After washing with cold 70 % ethanol and drying, the sgRNA pellets were resuspended in 20µl DEPC-H_2O. Final RNA concentration and purity were determined by NanoDrop spectrophotometry using RNA-specific settings.

3.2.8 RNA gel electrophoresis

A 1.5 % agarose gel was prepared by dissolving one agarose tablet in 5 ml 10x MOPS buffer and 35.8 ml H_2O. The solution was heated in the microwave until the agarose was completely dissolved. After cooling down, 9.2 ml 37 % formaldehyde was added, the gel was poured and allowed to solidify at RT. RNAs were mixed with an equal amount of RNA-loading dye, heated at 70 °C for 10 min and immediately incubated on ice for 3 min. The prepared RNA was loaded on the gel and the gel was run with 1x MOPS as running buffer.

3.2.9 Mutation of *tet3* alleles in *N.furzeri* via CRISPR-Cas9 microinjection

For *in vivo* application, fertilized one-cell stage embryos of the short-lived GRZ strain of *Nothobranchius furzeri* were collected shortly after spawning by fish facility staff. The purified sgRNAs, which were designed and provided by H.Mörl were combined with Cas9 mRNA and EGFP mRNA (Table 24) to allow later detection of successfully injected embryos. Additionally, phenol red (0.05% final concentration) was added to the injection mix to aid visual control during the procedure.

Table 24: Injection mix for CRISPR/Cas9-mediated *tet3* knockout.

Volume	**Material**
5 ng/µl	First sgRNA
5 ng/µl	Second sgRNA
100 ng/µl	Cas9 mRNA
50 ng/µl	EGFP mRNA
1 µl	Phenol red
Fill up to total Volume of 10 µl	DEPC-treated H_2O

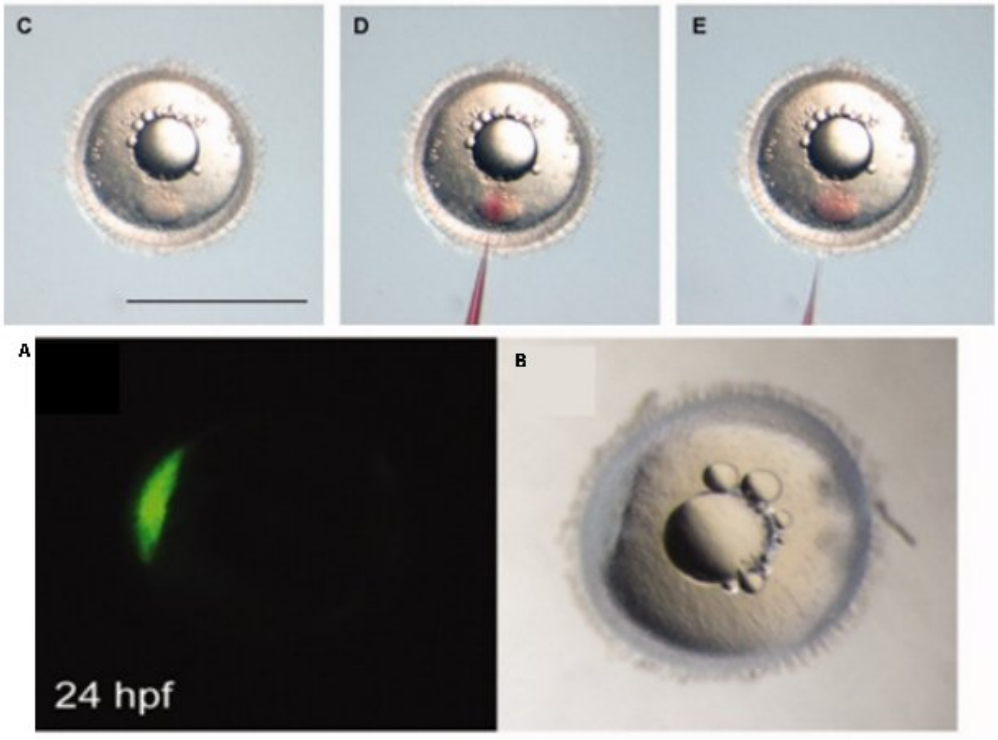

Figure 12 Microinjection (A,B) optimal EGFP signal after 24 h under a fluorescent microscope and embryo in blastula stage (adapted from Wourms, 1972). **(C-E)** Microinjection into single cell embryo (adapted from Hartmann and Englert, 2012 [39])

Microinjections were performed under a stereomicroscope using borosilicate glass needles pulled to fine tips with a programmable puller. Embryos were immobilized in small 1.5% agarose pockets filled with Danieau's buffer in petri dishes to restrict movement during injection. Injection volumes of approximately 1–2 nL were delivered directly into the cytoplasm as soon as possible after fertilization and before the first cleavage, following a microinjection protocol adapted specifically for *N. furzeri*, including penetration of the thick chorion as described by Hartmann & Englert [39].

After injection, embryos remained in the agarose pockets for 24 h, incubated at 30 °C, and were screened using the Zeiss SteREO Discovery.V8 microscope applying the setting for EGFP signal detection to distinguish successfully injected embryos from unsuccessfully injected ones (see Figure 12). EGFP-positive embryos were transferred to 96-well plates filled with Danieau's buffer for further incubation at 30 °C. A dozen non-injected embryos and injected embryos lacking EGFP signal were retained as experimental controls. Survival and developmental progression were monitored daily to assess early phenotypic effects, potential lethality linked to *tet3* disruption, injection-related stress, or general egg quality.

Following microinjection and incubation, putative founder embryos (F0 generation) were screened to confirm successful editing of the *tet3* locus. Genomic DNA was extracted from tail fin biopsies (fin clips) or whole embryos after lysis as described in chapter 3.2.3 and samples were analyzed via genotyping (3.2.2.2) and sexing PCR (3.2.2.1).

PCR products obtained from genotyping were purified and submitted to Eurofins Genomics for Sanger sequencing to identify indels introduced by non-homologous end joining (NHEJ). Founder fish carrying frameshift or nonsense mutations predicted to disrupt *tet3* protein function were selected for further breeding.

Throughout this process, embryos and juveniles were kept under standard *N. furzeri* husbandry conditions, and phenotypic observations were systematically documented to detect developmental abnormalities, reduced viability, or morphological changes potentially associated with *tet3* disruption. To reduce mosaicism, eliminate possible off-target mutations, and secure germline transmission of the desired mutation, founder animals were crossed with wild-type fish. This approach enables the establishment of a stable knockout line and facilitated the identification of homozygous mutants in subsequent generations.

Offspring from these crosses (F1 generation) were again screened at black-eyed stage for the presence of targeted mutations using the previously described genotyping strategy. Purified PCR amplicons were again sequenced by Sanger sequencing, and chromatograms were analyzed with dedicated software tools (TIDE [43] and ICE [44]) to characterize the precise mutation types and quantify editing efficiency.

3.2.10 cDNA Synthesis

Up to 500 ng of total RNA per sample were used for cDNA synthesis. Reverse transcription was performed with the Bio-Rad iScript™ Select cDNA Synthesis Kit according to the manufacturer's protocol. The resulting cDNA was stored at −20 °C until further use.

3.2.11 Reverse transcriptase quantitative PCR (RT-qPCR)

RT-qPCR analyses were conducted using the Bio-Rad CFX384 Real-Time PCR system with 384-well plates. Each reaction contained up to 5 ng/µl of cDNA. Reaction master mixes were prepared following established protocols [45], and a serial dilution of cDNA (1:2, 1:4, 1:8, and 1:16) was included to assess amplification efficiencies for each assay. Negative controls included a no-template control (water) and a no-reverse-transcriptase control (-RT) to detect

potential genomic DNA contamination. All samples and controls were analyzed in technical triplicates. The qPCR cycling parameters are shown in Table 25.

Table 25: RT-qPCR mix (left) and amplification program (right)

Volume	Material
5 µl	SYBR Green ER
0.2 µl	forward primer
0.2 µl	reverse primer
1.6 µl	nuclease free H_2O

Temperature	Time	Cycles
50 °C	2 min	
95 °C	10 min	
95 °C	15 sec	40
60 °C	20 sec	
60 °C	40 sec	
Followed by melting curve analysis		
95 °C	1 min	
55 °C	1 min	
55 °C	0,5 °C/s	
95 °C		
10 °C	8 min	

Data analysis was carried out using a custom Excel template provided by A.Richter implementing a PCR efficiency-corrected ΔΔCt calculation. Statistical comparisons between groups were performed using one-way ANOVA with Tukey's post hoc test. Graphical data presentations were generated using bioRender Graph.

$$\Delta Ct = \tilde{C}t_{ref.\,cond.} - Ct_{sample}$$

Equation 1 Equation to calculate ΔCt values for RT-qPCR

$$FC = \frac{E_{gene}^{(\Delta Ct_{gene})}}{\sqrt[2]{E_{ref.\ gene\,1}^{(\Delta Ct_{ref.\ gene\,1})} \times E_{ref.\ gene\,2}^{(\Delta Ct_{ref.\ gene\,2})}}}$$

Equation 2 Equation to calculate the FC with two reference genes.

3.2.12 Molecular Cloning

For molecular cloning, restriction digests with *NehI-HF* and *EcoRI-HF* were carried out to linearize vector backbones and prepare DNA inserts. Typically, around 1000 ng of PCR product or plasmid DNA was incubated with the appropriate restriction endonucleases and the corresponding reaction buffer in a total volume of 20–50 µl. Digests were performed at 37 °C for one to several hours, depending on enzyme requirements and fragment size. After completion, DNA fragments were separated by agarose gel electrophoresis, bands were cut out and purified using the DNA gel extraction kit (Macherey-Nagel).

Purified inserts and linearized vectors were ligated using *T4 DNA ligase*. Standard ligation reactions were set up in a volume of 20 µl, containing a molar insert-to-vector ratio of approximately 5:1 and ligase buffer. Incubation was usually performed overnight at 4 °C to maximize ligation efficiency. Following ligation, reaction mixtures were either directly transformed into competent *E. coli* cells (see 3.2.14) or stored in a -20°C fridge.

3.2.13 Transformation of *E. coli*

For transformation, chemically competent and electrocompetent *E. coli* cells were used, depending on plasmid size and type. After overnight ligation, reaction mixtures were left at room temperature for 30 min before transformation. For heat shock transformation, 5 µl of the ligation mix were gently combined with chemically competent *E. coli* TOP10 cells and incubated on ice for 30 min, followed by a brief heat shock at 42 °C for 40 seconds. Cells were then immediately returned to ice for 2 min. 250 µl of SOC medium were added and incubated at 37 °C with shaking (400 rpm) for 1 hour to allow recovery.

For electroporation, 1 µl of the ligation mix was added to 20 µl of electrocompetent *E. coli* Stable4 cells in pre-chilled electroporation cuvettes. The cells were pulsed under standard conditions (1.2 kV, 25 µF, 200 Ω), after which the cuvette was rinsed with 1 ml SOC medium. The suspension was transferred to a fresh 1.5 ml microcentrifuge tube and incubated at 37 °C with shaking (400 rpm) for 1 hour. Afterwards, the culture was centrifuged for 5 min at 5000 × g, 750 µl of supernatant were carefully removed, and the pellet was gently resuspended in the remaining 250 µl of medium.

Cells from either transformation approach were plated on LB agar containing the appropriate antibiotic and incubated overnight at 37 °C. On the following day, single colonies were picked

for screening by colony PCR to verify the presence and orientation of the insert, followed by plasmid isolation (3.2.5).

3.3 Fish handling

All routine handling of fish was performed by trained staff at the central animal facility, in accordance with FELASA recommendations for laboratory fish care. To ensure animal welfare and to detect early signs of distress or disease, fish were regularly scored based on external parameters such as skin integrity, fin condition, swimming behavior, and general appearance. Feeding was carried out with blood worms (*Chironomidae* larvae).

For the purpose of molecular genotyping, a small fragment of the caudal fin was removed (fin clip) under anesthesia to obtain DNA for downstream PCR-based analyses. Anesthesia was induced using the standard fish anesthetic tricaine methane sulfonate at a concentration of 200 mg/L. Fish were transferred individually into an anesthetic bath, where sedation occurred typically within 1–3 min. Once immobilized, each fish was placed on a Petri dish, photographed and a small section of the caudal fin was cut with a sterile scalpel. Following the procedure, fish were placed in fresh system water and monitored until full recovery, usually within 2–3 min [46].

4. Results

4.1 *dnmt* expression dynamics at the RNA level

To investigate age and tissue related dynamics of DNA methylation machinery in *Nothobranchius furzeri*, quantitative PCR analyses was performed. This included the four identified DNA methyltransferases (DNMT1, DNMT3aa, DNMT3ab, DNMT3ba) in *Nothobranchius furzeri* across three age groups (young, adult, old) and three tissues (gut, brain, gonads) in both sexes. Distinct expression trends were observed among the different DNMT paralogs and tissues.

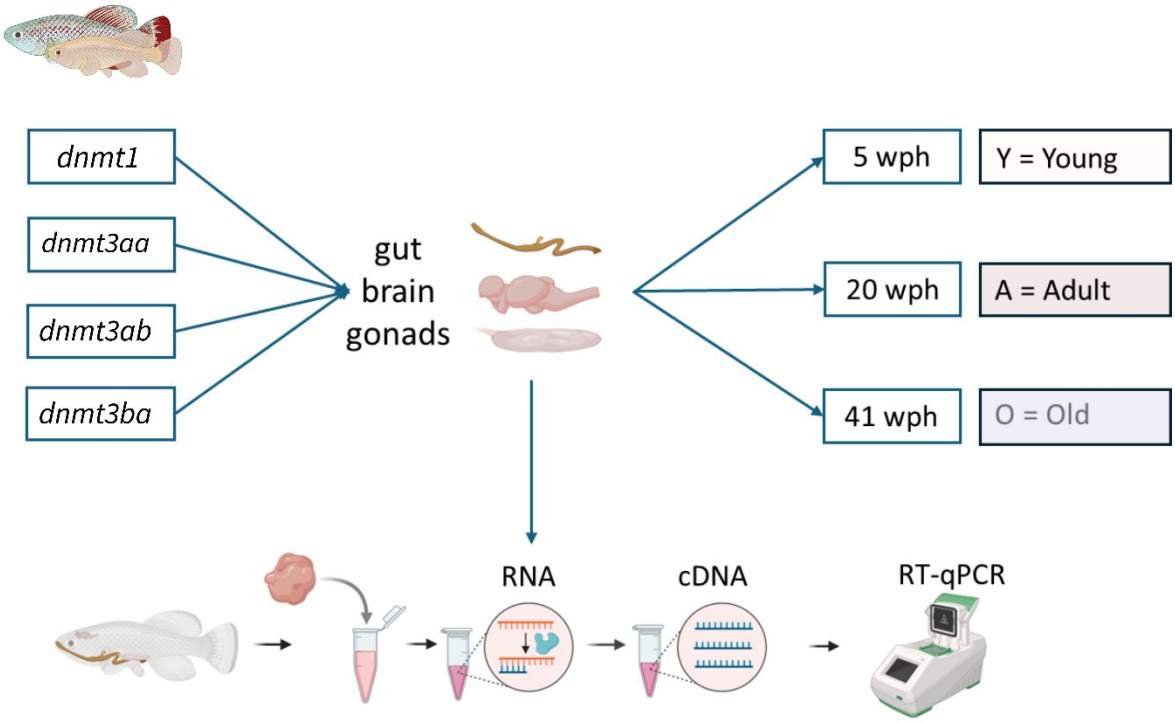

Figure 13 Overview of DNMT sampling and workflow. To assess the expression patterns of the four DNMT paralogues in *N. furzeri* (M08), organ samples were collected from gut, brain, and gonads of both males and females at three ages: young (5 wph), adult (20 wph), and old (41 wph). RNA was then isolated, reverse-transcribed into cDNA, and subsequently used for RT-qPCR analysis.

In the gut, expression levels were largely comparable between sexes in young and adult stages, whereas in old individuals males exhibited significantly higher DNMT expression than females (Figure 14 C,F,I,L). In the brain (Figure 14 B,E,H,K), no consistent sex- or age-specific pattern was detectable, although some variation occurred among paralogs and across age classes, these changes were irregular and not systematically maintained. In contrast, the gonads (Figure 14 A,D,G,J) showed a strong and consistent sex bias, with males displaying higher expression levels of all DNMTs across all age groups. While the level of statistical significance varied among paralogs, the overall male-biased expression pattern was robust. Interestingly, expression in adults was generally higher compared to young and old individuals, although not always reaching high significance. Across tissues DNMT1 (Figure 14 A-C) exhibited a pronounced upregulation in old males compared to old females, representing a significant sex-specific divergence in late life.

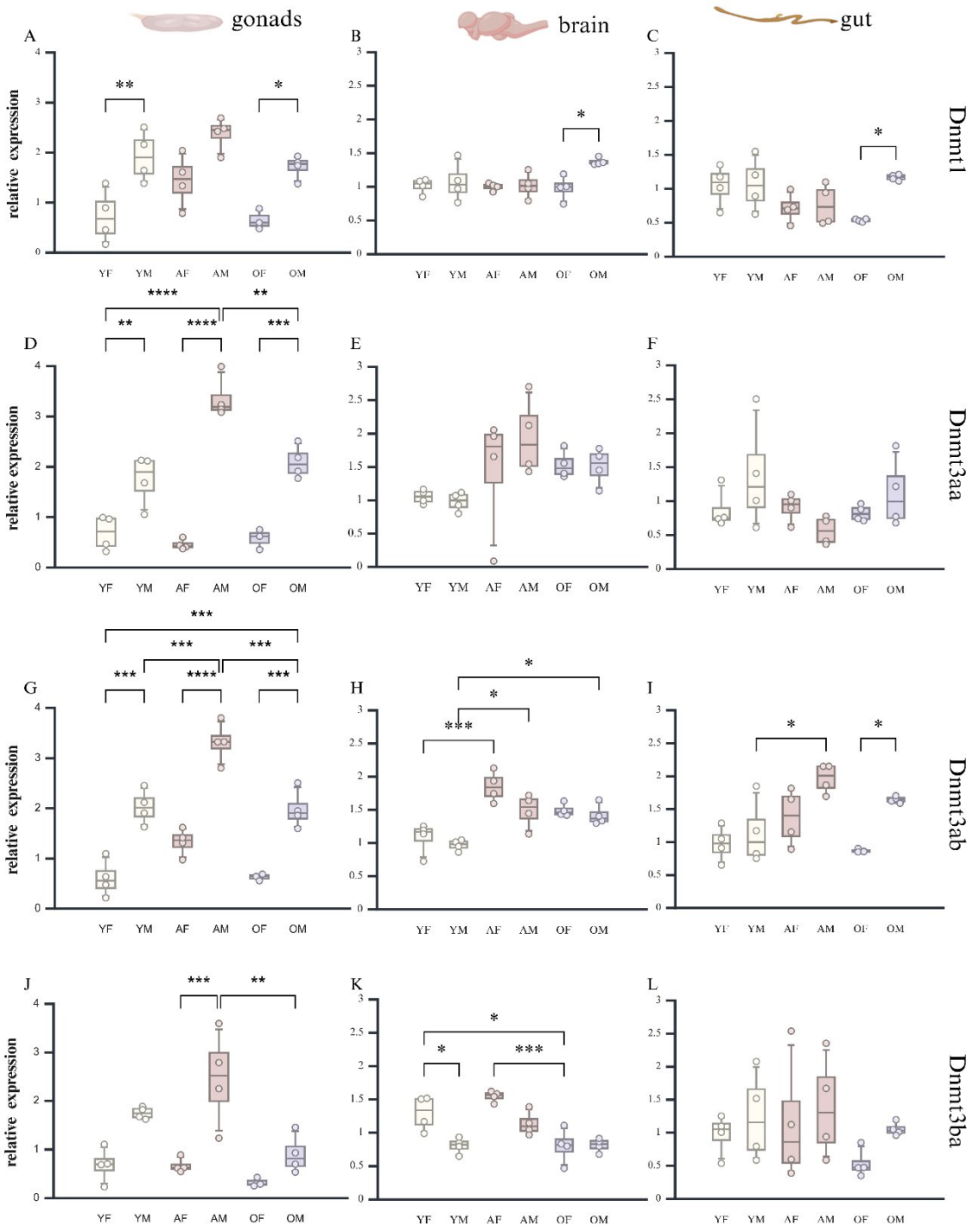

Figure 14 Tissue- and age-specific *dnmt* expression in *N. furzeri* males and females. In the gut (C, F, I, L), expression was largely comparable between sexes in young and adult stages, but old males showed significantly higher levels than females. In the brain (B, E, H, K), no consistent sex- or age-specific pattern was observed; minor variations among paralogs were irregular and not systematically maintained. In contrast, the gonads (A, D, G, J) displayed a strong male-biased expression across all age groups. Expression in adults was generally higher than in young or old individuals, though not always statistically significant. Notably, DNMT1 (A–C) exhibited pronounced upregulation in old males compared to old females, highlighting a clear sex-specific divergence in late life. Data are presented as mean ± SEM. Statistical significance was assessed using a one-way ANOVA ($F(5,17) = 40.78$, $p < 0.0001$, $\eta^2 = 0.923$) followed by Tukey's multiple comparisons test. ***$p < 0.0001$. All statistical analyses were performed in R (version 4.2.2). Asterisks indicate significance levels: **** = $p < 0.0001$.

4.2 Mutation of *tet3* alleles in GRZ strain of *N.furzeri*

To generate *tet3* mutants in the GRZ strain of *N. furzeri* 60 F0 embryos with a positive EGFP signal could be retained after injection (Figure 15). Of these, eight embryos hatched successfully, and five individuals survived to adulthood. Among those fish were 2 females and 3 males according to sex determination (Figure 16) and phenotype.

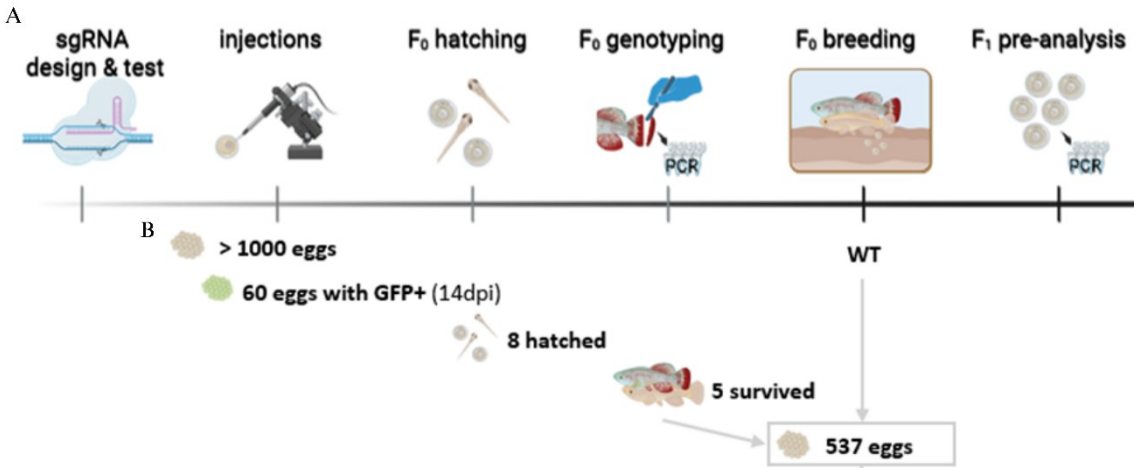

Figure 15 Workflow for generating *tet3* mutations in the GRZ strain of *N. furzeri* (A) Workflow of the procedure, including sgRNA preparation, microinjection, genetic analysis of embryos and adult fish, and outcrossing to produce the F1 generation. **(B)** Injection outcomes, including success and survival numbers.

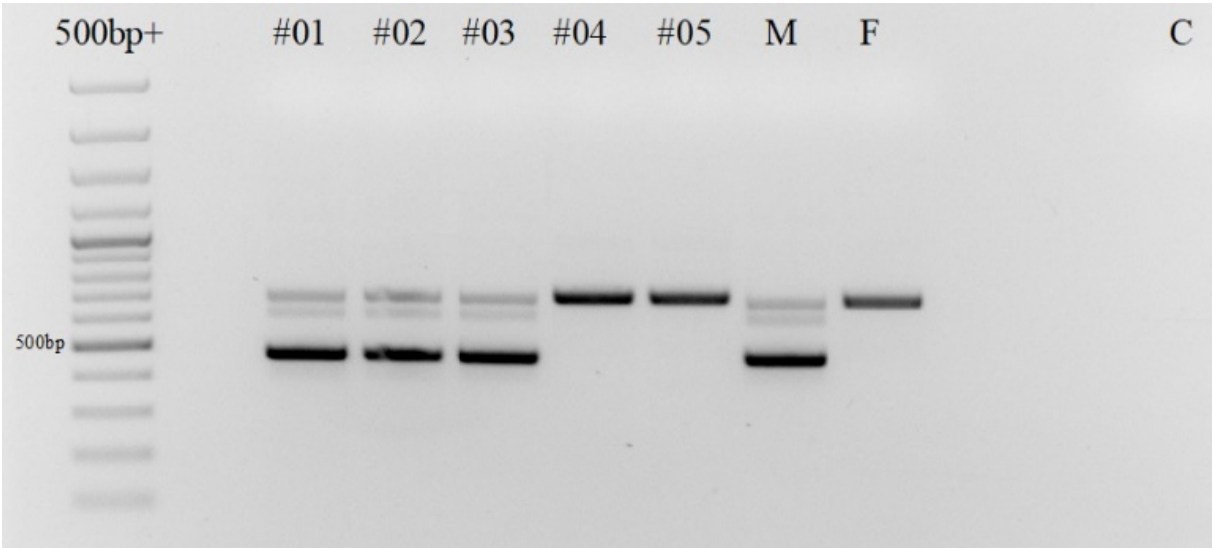

Figure 16 Results of sexing PCR. Results of the sexing PCR. Females show a single PCR product of 706 bp, whereas males additionally display a 465 bp PCR product.

These five fish were subsequently crossed with wild type partners, resulting in a total of 537 eggs in F1 generation. Following the established cultivation procedure, 77 eggs survived to the

black-eyed stage and were ready to hatch. It should be noted that the five breeding pairs produced highly variable quantities and qualities of eggs (see Table 27).

Table 26 Egg production and survival rates till hatching stage (absolute numbers and percentages) of the F1 generation

pair/sex	eggs	survived	[%]
Pair#1 ♂	144	26	18.05
Pair#2 ♂	114	10	8.77
Pair#3 ♂	226	26	11.5
Pair#4 ♀	30	8	26.6
Pair#5 ♀	23	7	30.43
∑	537	77	14.3

Due to logistical constraints, the project was discontinued at this point. Prior to termination, embryos were lysed and genotyped as described in 3.2.2.2. Genotyping PCR yielded results for 45 embryos, among which eight clear *knockouts* could be identified (see Figure 17 A-C). Since successful genotyping by PCR required both sgRNAs to cut simultaneously, an additional T7 assay was conducted. Out of 37 embryos tested with the T7 assay, 25 displayed indel formation (Figure 17 D,E). Furthermore, representative samples from each breeding pair (ten in total) were submitted for sequencing. ICE sequence analysis revealed variable indel patterns and *knockout* efficiencies, with approximately 40% of samples being heterozygotes and the remainder showing no detectable mutations (see Table 28).

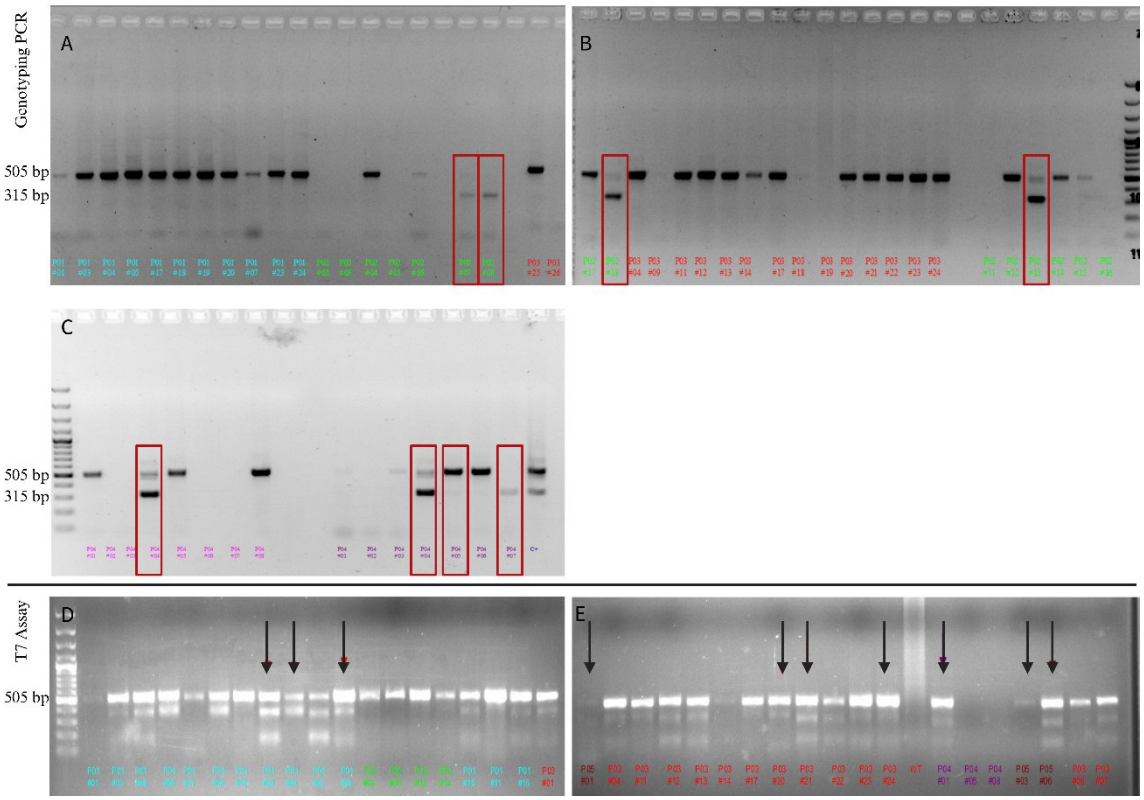

Figure 17 Analysis of *tet3* knockout candidates in GRZ. Results of **(A–C)** genotyping PCR showing 8 clear deletions (red squares). **(D, E) T7 assay** demonstrating indel formation in multiple samples. Ten of these samples were randomly selected for sequencing (black arrows).

Table 27 ICE analyses results

Sample	Indel [%]	KO-Score
GRZ_TET3_WT1	0	0
GRZ_TET3_P01_20	0	0
GRZ_TET3_P01_07	48	47
GRZ_TET3_P03_04	53	0
GRZ_TET3_P01_24	54	54
GRZ_TET3_P05_03	1	1
GRZ_TET3_P04_01	56	0
GRZ_TET3_P05_06	53	53
GRZ_TET3_P03_21	62	2
GRZ_TET3_P03_20	0	0
GRZ_TET3_P05_01	50	47

Analysis was performed using the ICE tool (Inference of CRISPR Edits). ICE compares Sanger sequencing traces of edited samples with a wild-type control and, based on regression modeling, calculates the proportion of insertions/deletions (Indel [%]) as well as the KO-score, which reflects the fraction of edits predicted to cause frameshifts or premature stop codons and thus likely result in loss of function.

4.3 Establishment of lentiviral transfection protocol in *N. furzeri* M08 cell lines

Pilot experiments using Lipofectamine-mediated transfection of cells with p300-pCS2 plasmid demonstrated efficient transgene delivery in HEK cells. In contrast, no detectable transfection was achieved in *Nothobranchius* cells under the same conditions. Neither direct transfection nor a 24-hour recovery period prior to transfection resulted in measurable expression of the transgene. Furthermore, supplementation with polybrene, a polycation that enhances viral particle binding to the cell membrane by neutralizing charge repulsion, did not improve transfection efficiency.

The initial lentiviral transduction experiments using the pLeGO-EGFP construct demonstrated the functionality of the system. Transduction efficiency was effective with 39% of cells expressing EGFP at a seeding density of 5 x 10^5 cells and 27% EGFP+ at 1 x 10^6 cells. EGFP expression was quantified using the Invitrogen Countess II FL Automated Cell Counter, which detects fluorescence intensity at the single-cell level to determine the proportion of EGFP-positive cells within the population. (Figure 18).

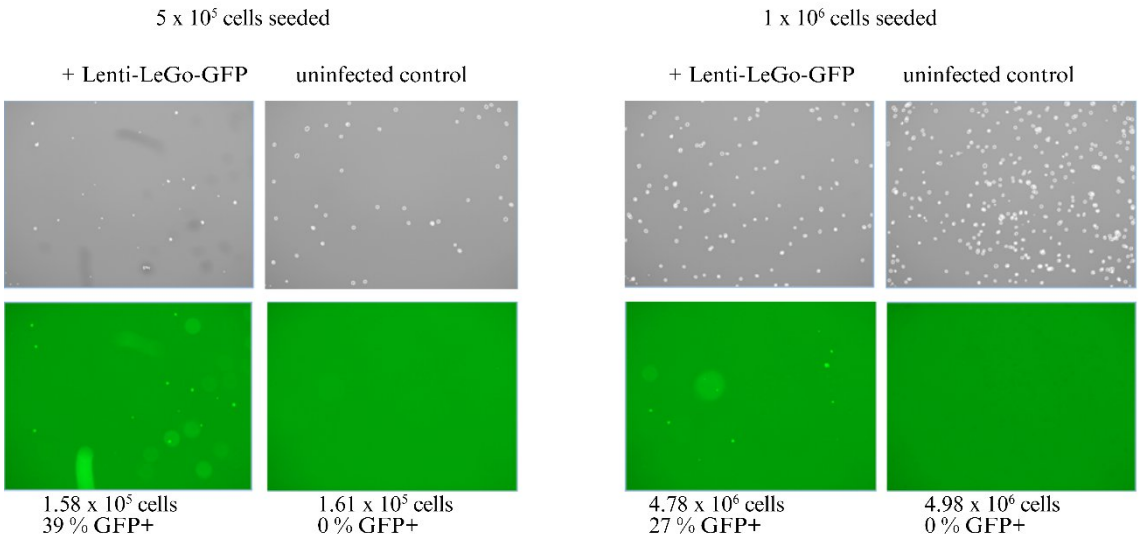

Figure 18 EGFP⁺ positive cells after pLeGO-EGFP lentiviral transduction in FiM-08 cells at different seeding densities. Initial experiments demonstrated the functionality of the lentiviral system and effective *EGFP* expression across tested conditions.

To determine the optimal viral load and to evaluate transduction efficiency in relation to viral dosage, a dilution series was performed in both HEK and *Nothobranchius* cells.

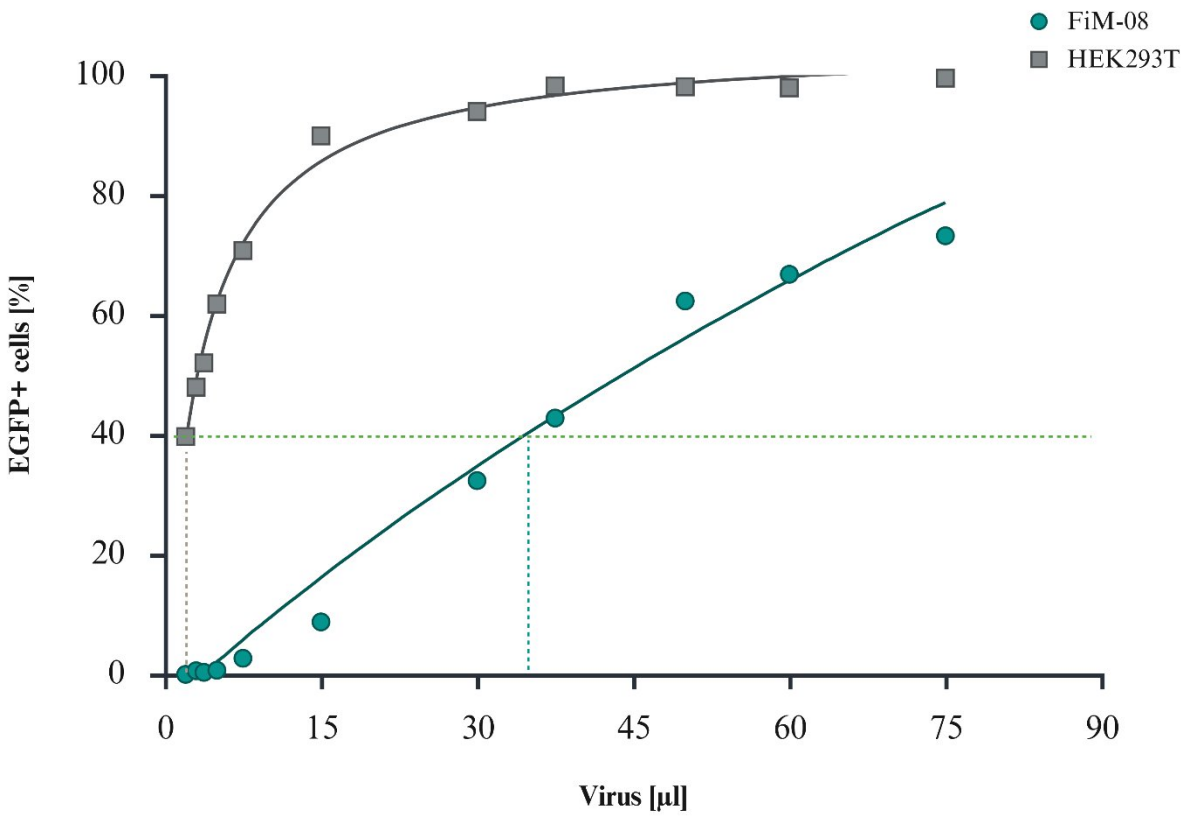

Figure 19 Dose-dependent EGFP⁺ response to pLeGO-EGFP lentiviral transduction in FiM-08 and HEK293T cells (FACS). The light green dashed line indicates an optimal transduction rate of ~40%. Grey and dark green lines show the virus volumes required to achieve this rate. A 4-parameter logistic regression (Hill slope = 1) was fitted; EC50 values were 196.2 (FiM-08) and 3.44 (HEK293T), with a strong fit ($R^2 > 0.98$).

For HEK293T cells, an optimal volume of approximately 2 µl of viral preparation was sufficient, whereas *Nothobranchius* cells required about 35 µl to achieve comparable results (see Figure 19 and Supplementary Table 1). Increasing the viral dose beyond this range may result in multiple integration events per cell, which is considered suboptimal. Although the precise viral titer was not determined, these experiments clearly demonstrated that transduction efficiency was substantially higher in HEK cells than in *Nothobranchius* cells, with the latter requiring approximately 10–15 times more virus to reach a similar level of transgene expression. Moreover, the results indicated that the transduction rate correlated positively with viral load.

The viral transduction was carried out using a dilution series of a newly prepared pLeGO plasmid containing the *tet1* coding sequence (construct details Figure 4). The objective was to determine an appropriate viral load for subsequent applications. Viral stocks were prepared in different concentrations for transduction of *Nothobranchius* cells, while HEK293T cells were included as controls and exposed to lower virus dosages, in accordance with the conditions established in the before mentioned experiment.

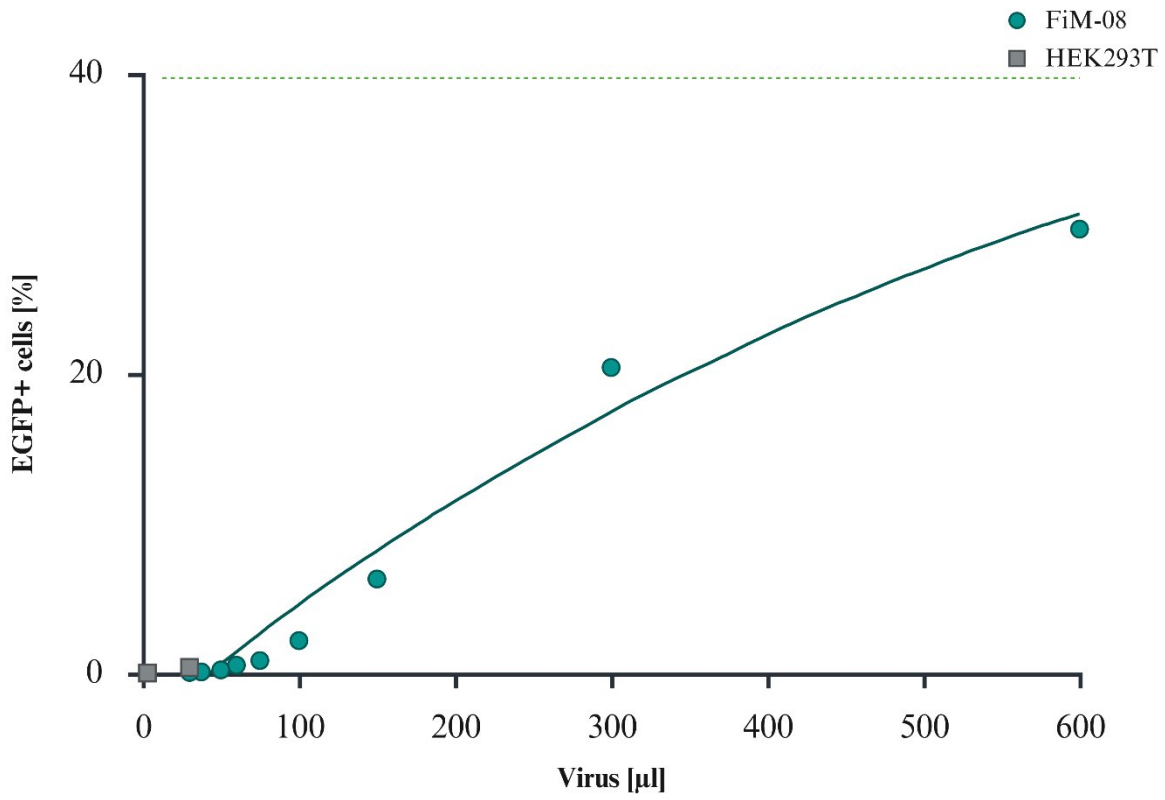

Figure 20 Dose-dependent EGFP⁺ response to pLeGO-EGFP lentiviral transduction in FiM-08 cells (FACS). A 4-parameter logistic regression (Hill slope = 1) was fitted; the EC50 value for FiM-08 was 943.5, with a strong fit ($R^2 = 0.975$).

FACS analysis of EGFP-positive, viable cells revealed patterns similar to the previous experiment. However, overall transduction efficiency was substantially lower in both HEK293T and *Nothobranchius* cells. In HEK293T cells, only 0.05% positivity was achieved with 3 µl of virus and 0.42% with 30 µl (see Supplementary Table 2). In *Nothobranchius* cells, transduction was even less efficient, with only 0.09% positivity at 30 µl and a maximum of ~30% even at the highest tested virus load of 600 µl. This reduction was anticipated, as the

LeGO vector size had nearly doubled, increasing from 7829 bp to 14304 bp. From this experiment, 170,000 EGFP-positive cells were sorted into a single well of a 12-well plate and subsequently cultivated. The gating strategy was optimized to minimize false-positive sorting and to reduce the risk of overgrowth by non-transduced cells (see Supplementary Figure 1). The data also indicated that transduction rates correlated positively with viral load. However, follow-up FACS analysis two weeks later failed to detect any EGFP signal, despite the cells being viable and proliferating. To verify whether the lentiviral construct had been successfully integrated, PCRs targeting *egfp* and the *tet1* exon - exon junction were performed (see Figure 20). The results confirmed the presence of the insert, thereby demonstrating successful transduction at the genomic level.

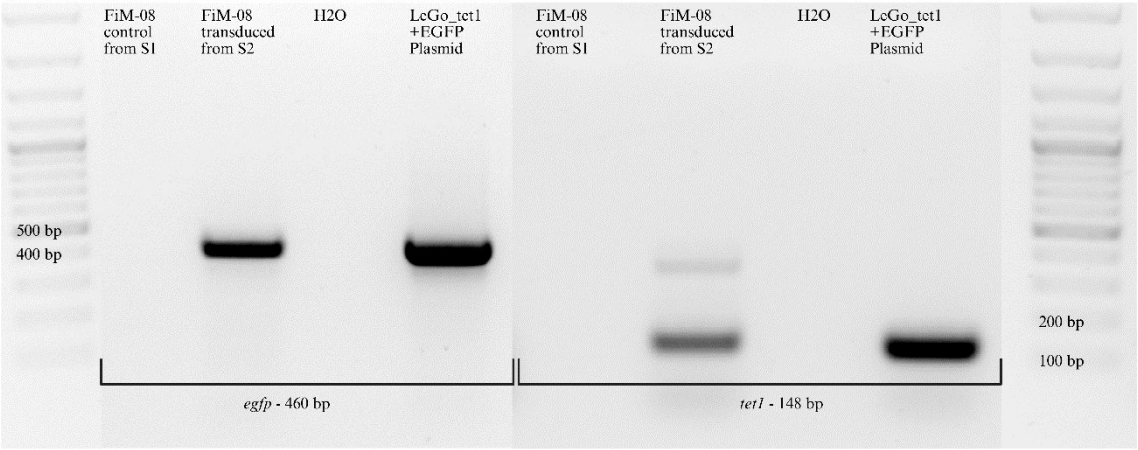

Figure 21 PCR validation of lentiviral transduction of pLeGO-EGFP-tet1 in FiM-08 cells. Amplification of EGFP and a *tet1* exon–exon junction. No specific amplicons were obtained from untransfected control cells (FiM-08 control S1), while the transfected cells and pLeGO-EGFP-tet1 display bands at the expected sizes. S1 and S2 refer to the biosafety levels of the laboratory. Lentviral experiments and its samples came for the S2 lab.

To further optimize efficiency, two additional experiments were conducted using substantially higher viral concentrations. For each attempt, fresh viral preparations were generated and applied exclusively to FiM-08 cells due to the limited supply of virus. Despite these modifications, the initial positive results could not be reproduced, and overall transduction rates remained extremely low at less than 0.1% (see Supplementary Table 3 & 4).

5. Discussion

5.1 *dnmt* expression patterns in *N. furzeri*

The quantitative PCR analyses conducted in this study revealed distinct expression patterns of the four identified DNA methyltransferases (*dnmt1, dnmt3aa, dnmt3ab, dnmt3ba*) across age groups and tissues in *N. furzeri*. While expression levels varied depending on tissue and developmental stage, several consistent features emerged that allow comparison with findings from other vertebrate models.

The most pronounced and robust trend was observed in the gonads, where all four DNMTs were consistently expressed at higher levels in males than in females across all age classes. This strong sex bias is in agreement with results from other teleost fish, including Nile tilapia and blackhead seabream, in which *dnmt3* paralogs display elevated expression in testes compared to ovaries [47,48]. The persistence of male-biased DNMT expression throughout the lifespan of *N. furzeri* suggests a conserved role of DNMTs in testis-specific epigenetic regulation. At the same time, the robustness of this pattern across all examined age groups appears more pronounced than in other species, which often report more dynamic changes in gonadal DNMT expression during sexual maturation or reproductive transitions [49]. In addition, a novel finding of this study was the upregulation of all DNMTs in adult gonads compared to both young and old stages - a pattern not previously described in the literature and apparently specific to this tissue. DNMTs may be involved in establishing and maintaining sex-specific gene expression patterns essential for reproductive function. For instance, adult gonads actively produce gametes, necessitating precise epigenetic regulation to maintain DNA integrity and proper gene expression during cell division. The upregulation of DNMTs could mediate these processes, as DNMTs play a role in maintaining epigenetic stability during gametogenesis by regulating DNA methylation patterns in germ cells. Another possibility is that elevated DNMT expression in adult gonads is linked to the regulation of sex differentiation and sexual maturation. Studies in medaka have shown that DNA methylation plays a critical role in gonadal differentiation and maintenance, with alterations in DNMT expression affecting gonadal development and function. [50]

By contrast, the expression profiles detected in the brain lacked clear sex- or age-related patterns. This stands in partial contrast to studies in rodents and humans, where *Dnmt1* and *Dnmt3a/b* are stably expressed in adult neurons and contribute to region-specific regulation of neural plasticity [51,52]. The absence of such consistent trends in *N. furzeri* may point to

species-specific regulatory mechanisms in neuronal tissues or reflect the rapid life history of this annual fish, in which neuronal *dnmt* regulation could follow a more transient trajectory.

In the gut, expression was largely comparable between sexes in young and adult stages, with significant male-biased expression emerging only in old individuals, this sex-specificity detected here appears to be a novel observation in *N.furzeri*.

Notably, across tissues, *dnmt1* showed a pronounced late-life upregulation in old males compared to old females, marking a unique sex-specific divergence that has not been widely described in other vertebrate models. This pattern may reflect interactions between sex, aging, and epigenetic maintenance mechanisms specific to the biology of *N. furzeri*.

Taken together, these findings indicate that *dnmt* expression in *N. furzeri* is both tissue-specific and sex-dependent, with a pronounced male bias in gonadal expression and a distinct late-life upregulation of dnmt1 in males. While these patterns broadly resemble those observed in other vertebrate models, they also reveal features that may be unique to the killifish. It is important to note, however, that the dynamics of epigenetic regulation remain poorly understood, and the temporal scale of such changes could significantly influence the interpretation of expression data. For example, *tet* expression has been shown to fluctuate markedly over the course of a single day in Chinese perch [53], suggesting that similar dynamics may affect *dnmt* expression. Indeed, one study reported that *dnmt* expression in the gonads of zebrafish follows a circadian rhythm, with peaks occurring at night in males and during the day in females.[54]

Moreover, DNMTs and TET enzymes act in opposing directions on the same substrate, suggesting a potential interdependence between their expression levels. From the perspective of energy balance, it could be hypothesized that the downregulation of one system may facilitate the upregulation of the other. This assumption could not be verified in the present study, as comparison with *tet* expression patterns across the same tissues and life stages (unpublished data) did not provide clear evidence. The broader epigenetic landscape is inherently complex, shaped by numerous interacting factors [55]. For example, it has been proposed that the physical presence of Tet proteins - particularly at unmethylated promoters - may impede DNMT-mediated deposition of 5-methylcytosine, thereby indirectly modulating methylation patterns [56]. Nevertheless, such observations remain limited, and additional evidence is required before drawing firm conclusions about potential mechanistic interference between the DNMT and TET families.

5.2 Feasibility and challenges of generating a *tet3* mutation in *N. furzeri*

The *knockout* experiments carried out in this study demonstrate that a targeted disruption of *tet3* in the short-lived *Nothobranchius furzeri* GRZ strain is, in principle, feasible. Despite several limiting factors, including suboptimal egg quality in two of the injections successful editing was achieved. The GRZ strain is a highly inbred line, and its limited genetic diversity and potentially reduced viability may have acted as confounding factor. Approximately two thirds of the injections were compromised either by technical limitations or by the quality of the starting material. Nevertheless, eight clear mutations could be confirmed, and additional embryos displayed measurable Indel formation. These results indicate that the generation of a stable *tet3* knockout in the GRZ line is achievable if procedures are optimized and larger injection series are conducted from the outset.

The experiments also revealed notable challenges that must be addressed in future work. A high level of embryo and larval mortality was observed in injected clutches. While this outcome can partly be attributed to handling stress and technical refinement during early injections, a biological contribution from *tet3* depletion cannot be excluded. Previous studies in vertebrates, particularly mice, have shown that *tet3* deficiency can impair development and survival [57–59] . Although direct evidence in fish is limited, similar trends of increased mortality have been reported in CRISPR-based *knockouts* of developmental regulators in zebrafish and medaka [60,61], suggesting that such effects may not be species-specific. These findings underscore the need for careful evaluation of survival across subsequent generations to distinguish technical mortality from biological effects linked to *tet3* loss.

Another important consideration is the presence of mosaicism in the injected generation, a common feature of CRISPR/Cas-based editing in teleosts [62]. ICE analysis confirmed, despite clear mutations, mixed Indel signatures, which is consistent with variable editing efficiencies within single embryos. Establishing a true homozygous line will therefore require further screening of F1 and later generations. Using alternative CRISPR/Cas variants, such as heiCas9 [63] may enhance *knockout* efficiency further and help mitigate mosaicism [64].

Taken together, the findings of this thesis demonstrate that generating a *tet3 knockout* line in the GRZ strain of *N. furzeri* is both feasible and promising. Despite some challenges successful editing was achieved, providing a solid foundation for future work. Establishing a stable *knockout* line will require optimization of injection handling, improved egg quality and

availability, and sufficient replicates to compensate for observed losses. Beyond technical considerations, a *tet3* knockout line offers significant opportunities to study the role of TET3 in DNA demethylation, tissue-specific gene regulation, and epigenetic homeostasis during development and aging. It also provides a platform to explore interactions with DNMTs, compensatory epigenetic mechanisms, and age-related phenotypes such as lifespan, reproductive fitness, and cellular plasticity.

5.3 Optimizing lentiviral transduction of killifish cells

Usually, viruses achieve higher efficiency and more stable transgene expression than lipofectamine, especially in hard-to-transfect cells. Additionally, direct transfection of plasmids into *Nothobranchius* cells by lipofection proved ineffective, whereas lentiviral delivery of an EGFP reporter plasmid resulted in robust and dose-dependent expression. Incorporation of the *tet1* coding sequence, however, reduced transduction efficiency, most likely because the viral genome exceeded the optimal packaging size by nearly 5 kb. Additional factors such as promoter silencing may have contributed to this reduction. The Spleen Focus-Forming Virus (SFFV) promoter, although widely used for strong constitutive expression in mammalian cells, is known to be prone to epigenetic repression. Evidence from murine experiments indicates that viral promoters can lose activity over time, likely through methylation-based mechanisms [65]. Given the short lifespan and pronounced age-related epigenetic drift in *Nothobranchius furzeri*, promoter silencing may be particularly pronounced. Since the transgene remains present but transcriptionally inactive, replacing SFFV with fish-native promoters such as EF1α or β-actin - reported to drive more stable expression in mammalian cells [66,67] - represents a logical next step. Alternatively, inducible promoters such as HSP70 (Heat Shock Promoter), which have been shown to function in other fish species, could reduce silencing due to their transient activation. Insulator elements, such as cHS4 from the chicken β-globin locus, may further increase the probability of retroviral expression and mitigate silencing [68]. However, any modifications must consider the already large construct size [69]. For example, the *β-actin* promoter alone can reach up to 2 kb, potentially exacerbating transduction inefficiency, whereas insulator elements are smaller (~250 bp each, requiring placement on both sides for full insulation, totaling ~500 bp).

Overexpression of TET1 was shown to modify the epigenome in vertebrates, though the extent and functional consequences remain unclear. TET1 increases 5-hydroxymethylcytosine

(5hmC) levels and promotes locus-specific DNA demethylation. In mammalian cells, it has been implicated in maintaining pluripotency and active demethylation [70–72], and modest tumor suppressive effects have been reported in hematopoietic malignancies [73]. Conversely, TET1 overexpression can also exert detrimental effects, including impaired hippocampal-dependent memory in rodents [71,74], increased pain sensitivity (hyperalgesia) [75], and the activation of oncogenic programs in certain cancers [76,77]. Collectively, these findings demonstrate that while TET1 plays a pivotal role in regulating DNA methylation, its downstream phenotypic effects are highly context-dependent and complex. Accordingly, the reduced transfection efficiency observed in later experiments may in part reflect unknown adverse effects arising from excessively high TET1 activity in the cells.

Transduction efficiency in this study was clearly dose-dependent, although the viral titers were not quantified. This highlights the importance of optimizing the viral load to achieve high expression levels while minimizing cellular stress. Excessive viral doses can induce cytotoxic effects by triggering cellular stress responses, apoptosis, or necrosis. Additionally, lentiviruses rely on specific cellular receptors for entry, and an excess of viral particles may saturate these receptors, potentially reducing transduction efficiency. Overdosing can also result in multiple genomic integrations and subsequent overexpression of the transgene, which may further contribute to cellular toxicity. Given that the exact viral titer remains unknown, finding the optimal balance between efficient transduction and cellular tolerance is particularly challenging. The poor results of the last two experiments in this study emphasize the critical need to define the viral dose precisely for successful transduction outcomes.

Overall, these findings demonstrate that lentiviral overexpression of TET1 in *Nothobranchius* is technically feasible, even with an oversized construct. However, careful optimization of both promoter selection and viral titer will be essential to achieve stable and efficient expression in future studies.

5.4 *N.furzeri* as a model for epigenetic studies and cross-species insights

Nothobranchius furzeri offers many advantages as a model organism for aging research, particularly its short lifespan. However, findings from this species cannot be directly extrapolated to humans. Evolutionary divergence leads to differences in the strength and timing of gene expression, RNA production, and protein abundance between species, which can alter tissue-specific functions and overall metabolic interactions. Phyre2-based comparative domain analysis of *N.furzeri* TET proteins against known structures of TET orthologs from other model organisms revealed ~75% identity in the main catalytic domain, but considerably lower similarity in the DNA-binding domains (TET1: 57%, TET2: 17%, TET3: 12%), pointing to potential species-specific differences in protein function. (Supplementary Figure 2-4). A comparison of TET proteins in terms of overall size and the positioning of their major domains by SMART (Supplementary Figure 5) further highlights noticeable, though not pronounced, structural differences. These variations may indicate, but do not necessarily imply functional divergence between species.

Many teleost fish, including zebrafish (*Danio rerio*) and *N. furzeri*, can regenerate complex tissues such as heart, fin, retina, and even parts of the brain. Zebrafish cardiomyocytes, for instance, can proliferate after cardiac injury and restore functional tissue [78]. Early studies assumed that conserved molecular pathways regulating regeneration could be harnessed in humans as well. In reality, human cardiomyocytes possess only very limited regenerative capacity, and activation of homologous pathways (e.g., FGF, Wnt, TGF-β) results in minimal repair or can even worsen it [79]. Interventions effective in fish often fail in mammals due to fundamental differences in cell cycle regulation, fibrosis, and immune responses.

Overall, while *N. furzeri* remains an excellent model for fundamental aging research and assessment of TET and DNMT functioning, caution is required when interpreting and translating findings to humans.

6. Outlook

The results of this thesis provide insight into the dynamics of DNMTs and TET enzymes, a highly complex system that is not yet fully understood and requires further investigation. The generation of a stable *tet3* knockout line in the GRZ strain, while technically challenging, proved to be feasible. A renewed attempt with an increased number of injections is likely to improve success rates and could ultimately lead to the establishment of a stable line.

Regarding DNMTs, it would be valuable to extend the expression analyses to additional tissues and life stages. The same applies to TET enzymes, as a broader dataset covering different organs and developmental phases would provide a more comprehensive understanding of their regulation. In this context, particular attention should also be given to embryonic development, as studies in mice have already demonstrated highly dynamic and stage-specific expression patterns during early stages [80].

Furthermore, these future investigations should consider the unresolved question of how rapidly epigenetic changes can occur. It is plausible, if not likely, that circadian rhythms influence the up- and downregulation of DNMTs and TETs [53], which adds another regulatory layer to be addressed.

Finally, the lentiviral-induced overexpression experiments in cell culture presented here represent the first of their kind in *Nothobranchius furzeri*. With further optimization, including the use of alternative promoters and precise viral titer determination, subsequent experiments are expected to achieve higher efficiency and enable the successful establishment of a stable overexpression cell line. Beyond advancing research on TET enzymes, these approaches could establish lentiviral techniques as a reliable tool for functional studies in *N. furzeri*.

Such a platform would allow a broad range of downstream analyses to assess the functional consequences of overexpression. These could include RNA expression profiling, protein-level quantification via Western blotting, DNA methylation assays such as Bisulfite Conversion-Based Assays, and cell-based functional assays such as proliferation analyses e.g., EdU incorporation [81] and regeneration or scratch assays [82]. Together, these experiments would provide a comprehensive evaluation of the impact of TET overexpression on cellular function and epigenetic regulation.

7. Bibliography

1. Wang K, Liu H, Hu Q, Wang L, Liu J, Zheng Z, et al. Epigenetic regulation of aging: implications for interventions of aging and diseases. Sig Transduct Target Ther [Internet]. 2022 Nov 7 [cited 2025 July 18];7(1). Available from: https://www.nature.com/articles/s41392-022-01211-8

2. Benayoun BA, Pollina EA, Brunet A. Epigenetic regulation of ageing: linking environmental inputs to genomic stability. Nat Rev Mol Cell Biol. 2015 Oct;16(10):593–610.

3. Pal S, Tyler JK. Epigenetics and aging. Sci Adv [Internet]. 2016 July [cited 2025 July 18];2(7). Available from: https://www.science.org/doi/10.1126/sciadv.1600584

4. Johnson AA, Akman K, Calimport SRG, Wuttke D, Stolzing A, De Magalhães JP. The Role of DNA Methylation in Aging, Rejuvenation, and Age-Related Disease. Rejuvenation Research. 2012 Oct;15(5):483–94.

5. Yang J, Guo R, Wang H, Ye X, Zhou Z, Dan J, et al. Tet Enzymes Regulate Telomere Maintenance and Chromosomal Stability of Mouse ESCs. Cell Reports. 2016 May;15(8):1809–21.

6. Xu Q, Wang C, Zhou JX, Xu ZM, Gao J, Sui P, et al. Loss of TET reprograms Wnt signaling through impaired demethylation to promote lung cancer development. Proc Natl Acad Sci USA [Internet]. 2022 Feb 8 [cited 2025 July 20];119(6). Available from: https://pnas.org/doi/full/10.1073/pnas.2107599119

7. Rasmussen KD, Helin K. Role of TET enzymes in DNA methylation, development, and cancer. Genes Dev. 2016 Apr 1;30(7):733–50.

8. Xu W, Zhang X, Liang F, Cao Y, Li Z, Qu W, et al. Tet1 Regulates Astrocyte Development and Cognition of Mice Through Modulating GluA1. Front Cell Dev Biol [Internet]. 2021 Oct 28 [cited 2025 July 20];9. Available from: https://www.frontiersin.org/articles/10.3389/fcell.2021.644375/full

9. Towers AJ, Tremblay MW, Chung L, Li X lei, Bey AL, Zhang W, et al. Epigenetic dysregulation of Oxtr in Tet1-deficient mice has implications for neuropsychiatric disorders. JCI Insight [Internet]. 2018 Dec 6 [cited 2025 July 20];3(23). Available from: https://insight.jci.org/articles/view/120592

10. Montgomery T, Uh K, Lee K. TET enzyme driven epigenetic reprogramming in early embryos and its implication on long-term health. Front Cell Dev Biol [Internet]. 2024 Aug 1 [cited 2025 July 20];12. Available from: https://www.frontiersin.org/articles/10.3389/fcell.2024.1358649/full

11. Matuleviciute R, Cunha PP, Johnson RS, Foskolou IP. Oxygen regulation of TET enzymes. The FEBS Journal. 2021 Dec;288(24):7143–61.

12. Kołodziej-Wojnar P, Borkowska J, Domaszewska-Szostek A, Bujanowska O, Noszczyk B, Krześniak N, et al. Ten-Eleven Translocation 1 and 2 Enzymes Affect Human Skin Fibroblasts in an Age-Related Manner. Biomedicines. 2023 June 7;11(6):1659.

13. Takeshita K, Suetake I, Yamashita E, Suga M, Narita H, Nakagawa A, et al. Structural insight into maintenance methylation by mouse DNA methyltransferase 1 (Dnmt1). Proc Natl Acad Sci USA. 2011 May 31;108(22):9055–9.

14. Okano M, Bell DW, Haber DA, Li E. DNA Methyltransferases Dnmt3a and Dnmt3b Are Essential for De Novo Methylation and Mammalian Development. Cell. 1999 Oct;99(3):247–57.

15. Pop S, Enciu AM, Tarcomnicu I, Gille E, Tanase C. Phytochemicals in cancer prevention: modulating epigenetic alterations of DNA methylation. Phytochem Rev. 2019 Aug;18(4):1005–24.

16. Cheng Y, Sun M, Chen L, Li Y, Lin L, Yao B, et al. Ten-Eleven Translocation Proteins Modulate the Response to Environmental Stress in Mice. Cell Reports. 2018 Dec;25(11):3194-3203.e4.

17. Hack LM, Dick ALW, Provençal N. Epigenetic mechanisms involved in the effects of stress exposure: focus on 5-hydroxymethylcytosine: Table 1: Environ Epigenet. 2016 Aug;2(3):dvw016.

18. Caldwell BA, Li L. Epigenetic regulation of innate immune dynamics during inflammation. Journal of Leukocyte Biology. 2024 Mar 29;115(4):589–606.

19. Gonzalez EA, Liu Y, Wang D, Jeziorek M, Bandyopadhyay S, Rao A, et al. TET3-mediated DNA oxidation is essential for intestinal epithelial cell response to stressors. Proc Natl Acad Sci USA [Internet]. 2023 Sept 12 [cited 2025 July 20];120(37). Available from: https://pnas.org/doi/10.1073/pnas.2221405120

20. Niehrs C. Active DNA demethylation and DNA repair. Differentiation. 2009 Jan;77(1):1–11.

21. Jurkowski TP, Jeltsch A. On the Evolutionary Origin of Eukaryotic DNA Methyltransferases and Dnmt2. Lyko F, editor. PLoS ONE. 2011 Nov 30;6(11):e28104.

22. Lio CWJ, Yue X, Lopez-Moyado IF, Tahiliani M, Aravind L, Rao A. TET methylcytosine oxidases: new insights from a decade of research. J Biosci. 2020;45:21.

23. Iyer LM, Zhang D, De Souza RF, Pukkila PJ, Rao A, Aravind L. Lineage-specific expansions of TET/JBP genes and a new class of DNA transposons shape fungal genomic and epigenetic landscapes. Proc Natl Acad Sci USA. 2014 Feb 4;111(5):1676–83.

24. Liu J, Hu H, Panserat S, Marandel L. Evolutionary history of DNA methylation related genes in chordates: new insights from multiple whole genome duplications. Sci Rep. 2020 Jan 22;10(1):970.

25. Furness AI. The evolution of an annual life cycle in killifish: adaptation to ephemeral aquatic environments through embryonic diapause. Biological Reviews. 2016 Aug;91(3):796–812.

26. Zupkovitz G, Kabiljo J, Kothmayer M, Schlick K, Schöfer C, Lagger S, et al. Analysis of Methylation Dynamics Reveals a Tissue-Specific, Age-Dependent Decline in 5-

Methylcytosine Within the Genome of the Vertebrate Aging Model Nothobranchius furzeri. Front Mol Biosci. 2021 June 16;8:627143.

27. Valenzano DR, Benayoun BA, Singh PP, Zhang E, Etter PD, Hu CK, et al. The African Turquoise Killifish Genome Provides Insights into Evolution and Genetic Architecture of Lifespan. Cell. 2015 Dec;163(6):1539–54.

28. Genade T, Benedetti M, Terzibasi E, Roncaglia P, Valenzano DR, Cattaneo A, et al. Annual fishes of the genus *Nothobranchius* as a model system for aging research. Aging Cell. 2005 Oct;4(5):223–33.

29. Reichard M, Polačik M. Nothobranchius furzeri, an "instant" fish from an ephemeral habitat. Elife. 2019 Jan 8;8:e41548.

30. Blažek R, Polačik M, Kačer P, Cellerino A, Řežucha R, Methling C, et al. Repeated intraspecific divergence in life span and aging of African annual fishes along an aridity gradient: INTRASPECIFIC DIVERGENCE IN AGING. Evolution. 2017 Feb;71(2):386–402.

31. Cellerino A, Valenzano DR, Reichard M. From the bush to the bench: the annual *Nothobranchius* fishes as a new model system in biology. Biological Reviews. 2016 May;91(2):511–33.

32. Cui R, Willemsen D, Valenzano DR. Nothobranchius furzeri (African Turquoise Killifish). Trends in Genetics. 2020 July;36(7):540–1.

33. Baumgart M, Groth M, Priebe S, Savino A, Testa G, Dix A, et al. RNA-seq of the aging brain in the short-lived fish *N. furzeri* – conserved pathways and novel genes associated with neurogenesis. Aging Cell. 2014 Dec;13(6):965–74.

34. Li X, Wei W, Zhao QY, Widagdo J, Baker-Andresen D, Flavell CR, et al. Neocortical Tet3-mediated accumulation of 5-hydroxymethylcytosine promotes rapid behavioral adaptation. Proc Natl Acad Sci USA. 2014 May 13;111(19):7120–5.

35. Zupkovitz G, Kabiljo J, Kothmayer M, Schlick K, Schöfer C, Lagger S, et al. Analysis of Methylation Dynamics Reveals a Tissue-Specific, Age-Dependent Decline in 5-Methylcytosine Within the Genome of the Vertebrate Aging Model Nothobranchius furzeri. Front Mol Biosci [Internet]. 2021 June 16 [cited 2025 July 20];8. Available from: https://www.frontiersin.org/articles/10.3389/fmolb.2021.627143/full

36. Reichwald K, Petzold A, Koch P, Downie BR, Hartmann N, Pietsch S, et al. Insights into Sex Chromosome Evolution and Aging from the Genome of a Short-Lived Fish. Cell. 2015 Dec;163(6):1527–38.

37. Kirschner J, Weber D, Neuschl C, Franke A, Böttger M, Zielke L, et al. Mapping of quantitative trait loci controlling lifespan in the short-lived fish *Nothobranchius furzeri*– a new vertebrate model for age research. Aging Cell. 2012 Apr;11(2):252–61.

38. Valenzano DR. The short-lived African turquise killifish: am emerging experimental model for aging. Disease Models & Mechanisms. 2016 Feb 9;115–29.

39. Hartmann N, Englert C. A microinjection protocol for the generation of transgenic killifish (Species: *Nothobranchius furzeri*). Developmental Dynamics. 2012 June;241(6):1133–41.

40. Genome Editing: A Review of Literature. 1. Auflage. Saarbrücken: LAP LAMBERT Academic Publishing; 2018.

41. Richter A, Krug J, Englert C. Molecular Sexing of*Nothobranchius furzeri*Embryos and Larvae. Cold Spring Harb Protoc. 2022 Dec;2022(12):pdb.prot107782.

42. Ehrke-Schulz E, Bergmann T, Schiwon M, Doerner J, Saydaminova K, Lieber A, et al. Quantification of designer nuclease induced mutation rates: a direct comparison of different methods. Molecular Therapy - Methods & Clinical Development. 2016;3:16047.

43. Conant D, Hsiau T, Rossi N, Oki J, Maures T, Waite K, et al. Inference of CRISPR Edits from Sanger Trace Data. The CRISPR Journal. 2022 Feb 1;5(1):123–30.

44. Brinkman EK, Van Steensel B. Rapid Quantitative Evaluation of CRISPR Genome Editing by TIDE and TIDER. In: Luo Y, editor. CRISPR Gene Editing [Internet]. New York, NY: Springer New York; 2019 [cited 2025 Sept 2]. p. 29–44. (Methods in Molecular Biology; vol. 1961). Available from: http://link.springer.com/10.1007/978-1-4939-9170-9_3

45. Zhao F, Maren NA, Kosentka PZ, Liao YY, Lu H, Duduit JR, et al. An optimized protocol for stepwise optimization of real-time RT-PCR analysis. Hortic Res. 2021 Aug 1;8(1):179.

46. Ayala-Soldado N, Mora-Medina R, Molina-López AM, Lora-Benítez AJ, Moyano-Salvago R. Evaluation of the Effectiveness of Eugenol and MS-222 as Anesthetics in Zebrafish in Repeated Exposures and Post-Anesthesia Behaviour. Animals. 2024 Aug 21;14(16):2418.

47. Sun LX, Wang YY, Zhao Y, Wang H, Li N, Ji XS. Global DNA Methylation Changes in Nile Tilapia Gonads during High Temperature-Induced Masculinization. Wang H, editor. PLoS ONE. 2016 Aug 3;11(8):e0158483.

48. Wang F, Qin Z, Li Z, Yang S, Gao T, Sun L, et al. Dnmt3aa but Not Dnmt3ab Is Required for Maintenance of Gametogenesis in Nile Tilapia (Oreochromis niloticus). IJMS. 2021 Sept 21;22(18):10170.

49. Zhang Y, Sun X, Zhang L, Zhang W. Testicular Dnmt3 expression and global DNA methylation are down-regulated by gonadotropin releasing hormones in the ricefield eel Monopterus albus. Sci Rep. 2017 Feb 22;7(1):43158.

50. Ribas L, Vanezis K, Imués MA, Piferrer F. Treatment with a DNA methyltransferase inhibitor feminizes zebrafish and induces long-term expression changes in the gonads. Epigenetics & Chromatin. 2017 Dec;10(1):59.

51. Guintivano J, Aryee MJ, Kaminsky ZA. A cell epigenotype specific model for the correction of brain cellular heterogeneity bias and its application to age, brain region and major depression. Epigenetics. 2013 Mar;8(3):290–302.

52. Feng J, Zhou Y, Campbell SL, Le T, Li E, Sweatt JD, et al. Dnmt1 and Dnmt3a maintain DNA methylation and regulate synaptic function in adult forebrain neurons. Nat Neurosci. 2010 Apr;13(4):423–30.

53. Cheng J, Zhu X, Meng Y, Cheng C, Zeng W, Chen L, et al. Differential expression of Tet family genes and their potential role in regulating skeletal muscle development of Siniperca chuatsi. Aquaculture Reports. 2023 Apr;29:101486.

54. Paredes JF, Lopez-Olmeda JF, Muñoz-Cueto JA, Sánchez-Vázquez F. Circadian expression of DNA methylation and demethylation genes in zebrafish gonads. Chronobiology International. 2018 July 3;35(7):920–32.

55. Cariaga-Martínez AE, Gutiérrez KJ, Alelú-Paz R. The Vast Complexity of the Epigenetic Landscape during Neurodevelopment: An Open Frame to Understanding Brain Function. IJMS. 2018 May 1;19(5):1333.

56. Wu X, Zhang Y. TET-mediated active DNA demethylation: mechanism, function and beyond. Nat Rev Genet. 2017 Sept;18(9):517–34.

57. Inoue A, Shen L, Matoba S, Zhang Y. Haploinsufficiency, but Not Defective Paternal 5mC Oxidation, Accounts for the Developmental Defects of Maternal Tet3 Knockouts. Cell Reports. 2015 Feb;10(4):463–70.

58. Joshi K, Zhang L, Breslin S.J. P, Kini AR, Zhang J. Role of TET dioxygenases in the regulation of both normal and pathological hematopoiesis. J Exp Clin Cancer Res. 2022 Oct 7;41(1):294.

59. Li T, Yang D, Li J, Tang Y, Yang J, Le W. Critical Role of Tet3 in Neural Progenitor Cell Maintenance and Terminal Differentiation. Mol Neurobiol. 2015 Feb;51(1):142–54.

60. Yeh YC, Kinoshita M, Ng TH, Chang YH, Maekawa S, Chiang YA, et al. Using CRISPR/Cas9-mediated gene editing to further explore growth and trade-off effects in myostatin-mutated F4 medaka (Oryzias latipes). Sci Rep. 2017 Sept 12;7(1):11435.

61. Auer TO, Duroure K, De Cian A, Concordet JP, Del Bene F. Highly efficient CRISPR/Cas9-mediated knock-in in zebrafish by homology-independent DNA repair. Genome Res. 2014 Jan;24(1):142–53.

62. Yamanaka T, Sogo A, Maegawa S, Kinoshita M. Low-temperature embryo incubation suppresses off-target mutagenesis during CRISPR-Cas9 genome editing in medaka (Oryzias latipes) and zebrafish (Danio rerio). Transgenic Res. 2025 Dec;34(1):15.

63. Thumberger T, Tavhelidse-Suck T, Gutierrez-Triana JA, Cornean A, Medert R, Welz B, et al. Boosting targeted genome editing using the hei-tag. eLife. 2022 Mar 25;11:e70558.

64. Liu P, Luk K, Shin M, Idrizi F, Kwok S, Roscoe B, et al. Enhanced Cas12a editing in mammalian cells and zebrafish. Nucleic Acids Research. 2019 May 7;47(8):4169–80.

65. Herbst F, Ball CR, Tuorto F, Nowrouzi A, Wang W, Zavidij O, et al. Extensive Methylation of Promoter Sequences Silences Lentiviral Transgene Expression During Stem Cell Differentiation In Vivo. Molecular Therapy. 2012 May;20(5):1014–21.

66. Wang X, Xu Z, Tian Z, Zhang X, Xu D, Li Q, et al. The EF-1α promoter maintains high-level transgene expression from episomal vectors in transfected CHO-K1 cells. J Cellular Molecular Medi. 2017 Nov;21(11):3044–54.

67. Hong S, Hwang DY, Yoon S, Isacson O, Ramezani A, Hawley RG, et al. Functional Analysis of Various Promoters in Lentiviral Vectors at Different Stages of In Vitro Differentiation of Mouse Embryonic Stem Cells. Molecular Therapy. 2007 Sept;15(9):1630–9.

68. Rivella S, Callegari JA, May C, Tan CW, Sadelain M. The cHS4 Insulator Increases the Probability of Retroviral Expression at Random Chromosomal Integration Sites. J Virol. 2000 May 15;74(10):4679–87.

69. Sweeney NP, Vink CA. The impact of lentiviral vector genome size and producer cell genomic to gag-pol mRNA ratios on packaging efficiency and titre. Molecular Therapy - Methods & Clinical Development. 2021 June;21:574–84.

70. Gao Y, Chen J, Li K, Wu T, Huang B, Liu W, et al. Replacement of Oct4 by Tet1 during iPSC Induction Reveals an Important Role of DNA Methylation and Hydroxymethylation in Reprogramming. Cell Stem Cell. 2013 Apr;12(4):453–69.

71. Guo JU, Su Y, Zhong C, Ming G li, Song H. Hydroxylation of 5-Methylcytosine by TET1 Promotes Active DNA Demethylation in the Adult Brain. Cell. 2011 Apr;145(3):423–34.

72. Tahiliani M, Koh KP, Shen Y, Pastor WA, Bandukwala H, Brudno Y, et al. Conversion of 5-Methylcytosine to 5-Hydroxymethylcytosine in Mammalian DNA by MLL Partner TET1. Science. 2009 May 15;324(5929):930–5.

73. Cimmino L, Dawlaty MM, Ndiaye-Lobry D, Yap YS, Bakogianni S, Yu Y, et al. TET1 is a tumor suppressor of hematopoietic malignancy. Nat Immunol. 2015 June;16(6):653–62.

74. Rudenko A, Dawlaty MM, Seo J, Cheng AW, Meng J, Le T, et al. Tet1 Is Critical for Neuronal Activity-Regulated Gene Expression and Memory Extinction. Neuron. 2013 Sept;79(6):1109–22.

75. Pan Z, Zhang M, Ma T, Xue ZY, Li GF, Hao LY, et al. Hydroxymethylation of microRNA-365-3p Regulates Nociceptive Behaviors via Kcnh2. J Neurosci. 2016 Mar 2;36(9):2769–81.

76. Good CR, Panjarian S, Kelly AD, Madzo J, Patel B, Jelinek J, et al. TET1-Mediated Hypomethylation Activates Oncogenic Signaling in Triple-Negative Breast Cancer. Cancer Research. 2018 Aug 1;78(15):4126–37.

77. Shirai K, Nagae G, Seki M, Kudo Y, Kamio A, Hayashi A, et al. TET1 upregulation drives cancer cell growth through aberrant enhancer hydroxymethylation of HMGA2 in hepatocellular carcinoma. Cancer Science. 2021 July;112(7):2855–69.

78. Jopling C, Sleep E, Raya M, Martí M, Raya A, Belmonte JCI. Zebrafish heart regeneration occurs by cardiomyocyte dedifferentiation and proliferation. Nature. 2010 Mar 25;464(7288):606–9.

79. Działo E, Czepiel M, Tkacz K, Siedlar M, Kania G, Błyszczuk P. WNT/β-Catenin Signaling Promotes TGF-β-Mediated Activation of Human Cardiac Fibroblasts by Enhancing IL-11 Production. IJMS. 2021 Sept 17;22(18):10072.

80. Singh A, Rappolee DA, Ruden DM. Epigenetic Reprogramming in Mice and Humans: From Fertilization to Primordial Germ Cell Development. Cells. 2023 July 17;12(14):1874.

81. Biram A, Shulman Z. Evaluation of B Cell Proliferation in vivo by EdU Incorporation Assay. BIO-PROTOCOL [Internet]. 2020 [cited 2025 Sept 4];10(9). Available from: https://bio-protocol.org/e3602

82. Balko S, Kerr E, Buchel E, Logsetty S, Raouf A. A Robust and Standardized Approach to Quantify Wound Closure Using the Scratch Assay. MPs. 2023 Sept 17;6(5):87.

83. Kelley LA, Mezulis S, Yates CM, Wass MN, Sternberg MJE. The Phyre2 web portal for protein modeling, prediction and analysis. Nat Protoc. 2015 June;10(6):845–58.

84. Letunic I, Khedkar S, Bork P. SMART: recent updates, new developments and status in 2020. Nucleic Acids Research. 2021 Jan 8;49(D1):D458–60.

8. Supplement

Supplementary Table 1 Dose-dependent GFP$^+$ response to lentiviral transduction (Exp02) with pLeGO-EGFP in FiM-08 and HEK293T cells (FACS analysis)

Sample	#1	#2	#3	#4	#5	#6	#7	#8	#9	#10	#11	#12
Dilution	0	1:40	1:50	1:60	1:80	1:100	1:200	1:400	1:600	1:800	1:1000	1:1500
Medium + polybrene [µl]	3000	2925	2940	2950	2963	2970	2985	2993	2995	2996,3	2997	2998
Virus [µl]	0	75	60	50	37,5	30	15	7,5	5	3,75	3	2
HEK 293T GFP+ cells [%]	0	39,72	47,96	52,02	61,83	70,75	89,88	93,94	98,20	98,07	97,89	99,50
FiM-08 GFP+ cells [%]	0	0,06	0,66	0,39	0,75	2,74	8,81	32,38	42,81	62,34	66,78	73,21

Supplementary Table 2 Dose-dependent GFP$^+$ response to lentiviral transduction (Exp03) with pLeGO-EGFP in FiM-08 and HEK293T cells (FACS analysis)

Sample	#1	#2	#3	#4	#5	#6	#7	#8	#9	#10	#11
Dilution	0	1:5	1:10	1:20	1:30	1:40	1:50	1:60	1:80	1:100	1:1000
Medium + polybrene [µl]	3000	2400	2700	2850	2900	2925	2940	2950	2962.5	2970	2997
Virus [µl]	0	600	300	150	100	75	60	50	37.5	30	3
HEK 293T GFP+ cells [%]	0									0,42	0,05
FiM-08 GFP+ cells [%]	0	29,66	20,43	6,32	2,21	0,88	0,57	0,26	0,12	0,09	

Supplementary Table 3 Dose-dependent GFP$^+$ response to lentiviral transduction (Exp04) with pLeGO-EGFP in FiM-08 and HEK293T cells (FACS analysis)

Sample	#1	#2	#3	#4	#5	#6
Dilution	0	1:5	1:10	1:42.5	1:80	1:100
Medium + polybrene [µl]	3000	2400	2700	2929	2962.5	2970
Virus [µl]	0	600	300	71	37.5	30
HEK 293T GFP+ cells [%]	0	0	0	0	0	0
FiM-08 GFP+ cells [%]	0	0.05	0.06	0	0	0

Supplementary Table 4 Dose-dependent GFP$^+$ response to lentiviral transduction (Exp05) with pLeGO-EGFP in FiM-08 and HEK293T cells (FACS analysis)

Sample	#1	#2	#3	#4	#5
Dilution	0	1:1	1:3	1:10	1:30
Medium+polybrene [µl]	3000	1500	2000	2700	2900
Virus [µl]	0	1500	1000	300	100
FiM-08 GFP+ cells [%]	0	0	0	0.02	0.01

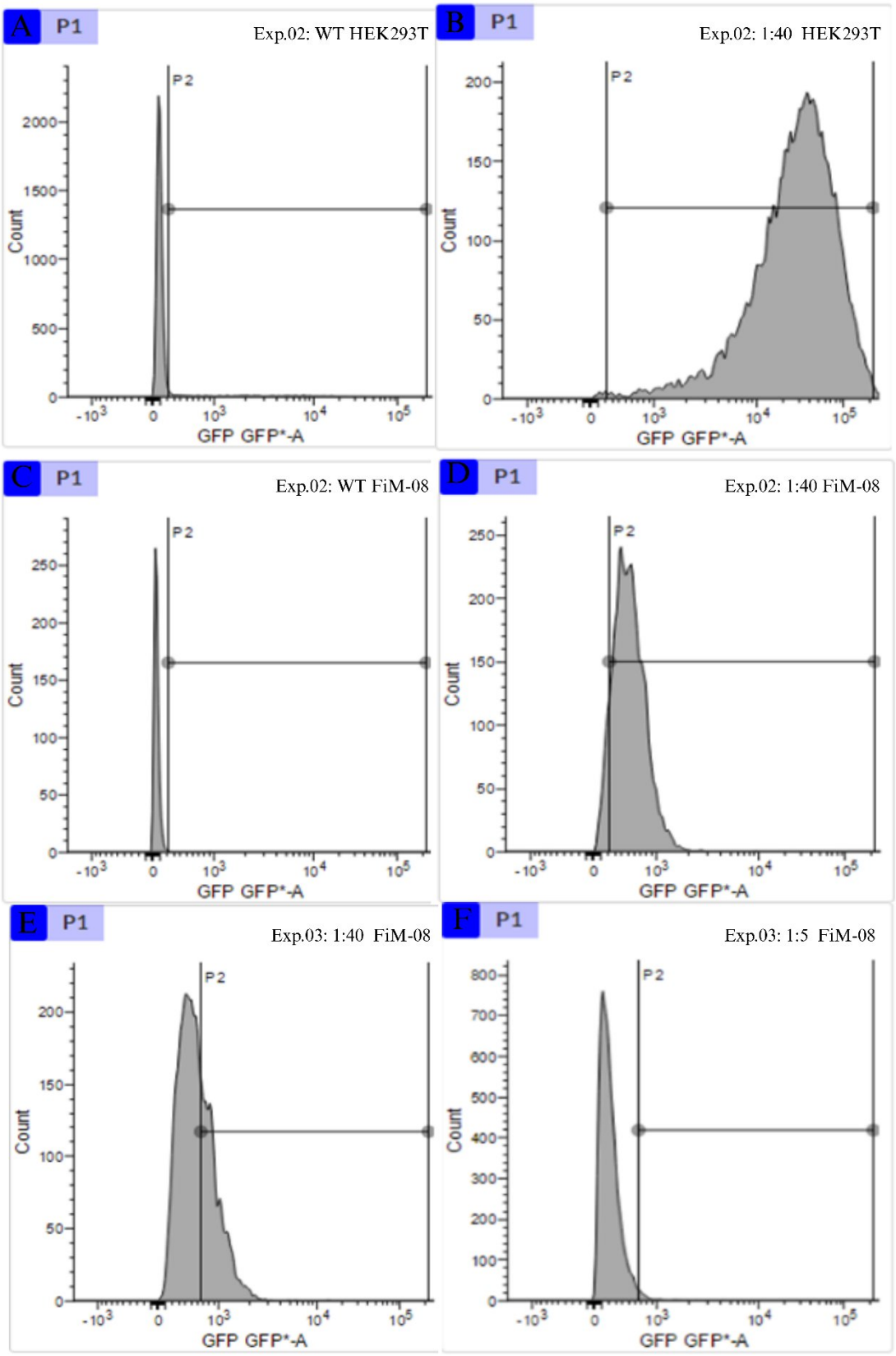

Supplementary Figure 1 Gating strategy for transfection experiments. (A) Assessment of GFP$^+$ background signal in HEK293T wild-type cells**. (B)** Gating defined after background assessment for a dilution series of 1 µl virus : 40 µl medium in HEK293T cells. **(C)** Assessment of GFP$^+$ background signal in FiM-08 wild-type cells. **(D)** Gating defined after background assessment for a dilution series of 1 µl virus in 40 µl medium in FiM-08 cells. **(E, F)** Example of gating applied to higher GFP$^+$ responses in FiM-08 cells (1:40 and 1:5 dilutions), demonstrating the strategy used to avoid false-positive sorting.

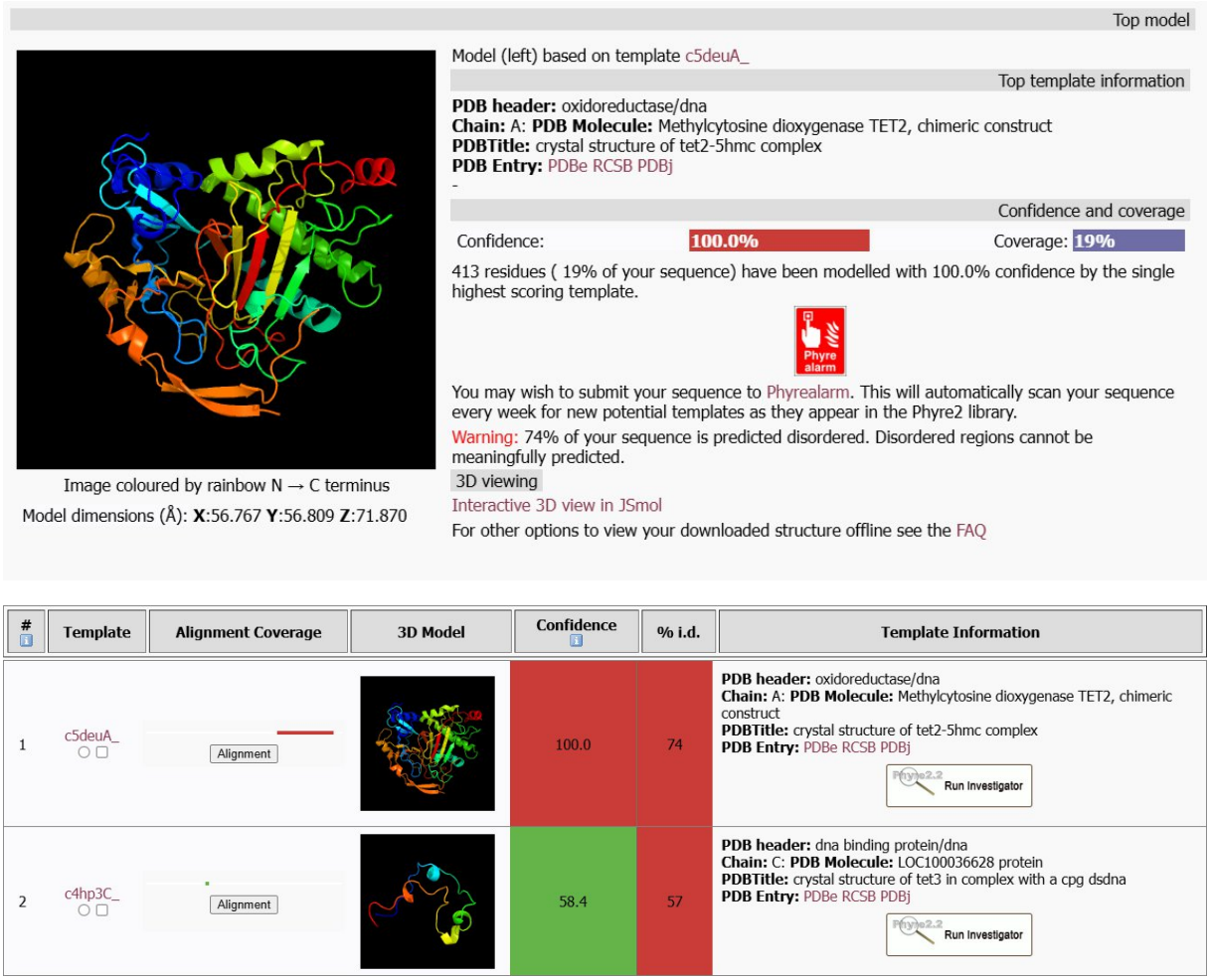

Supplementary Figure 2 Phyre2.2 homology modeling results for *N. furzeri* TET1 protein sequences. The analysis identified the crystal structure of human TET2 (PDB ID: 5DEU) as the top template with 100% confidence and 19% coverage and 74% of the main Domain to be identical between homologues with and confidence of 100 (Screenshots were obtained from the Phyre2 web portal, Kelley et al., 2015, [83]).

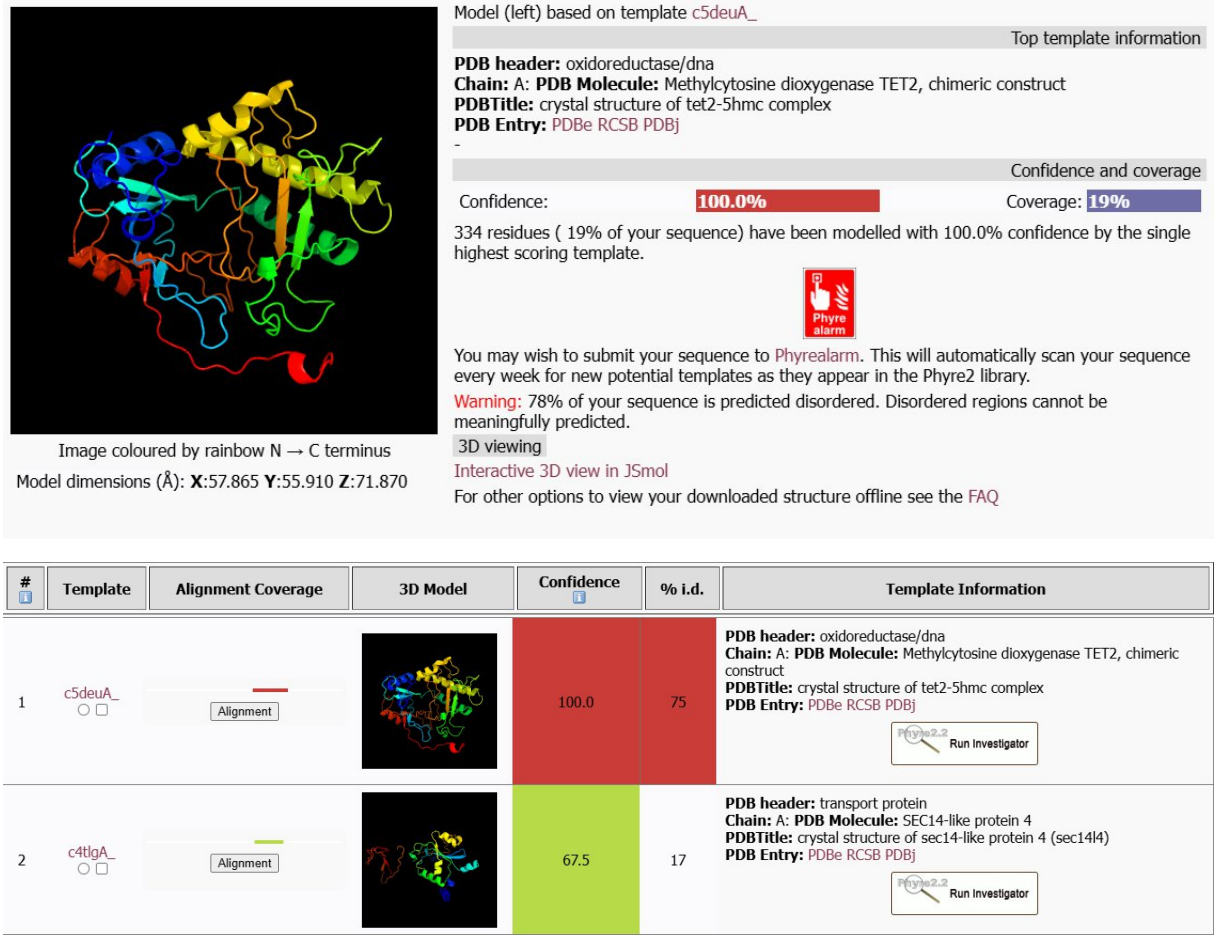

Supplementary Figure 3 Phyre2.2 homology modeling results for *N. furzeri* TET2 protein sequences. The analysis identified the crystal structure of human TET2 as the top template with 100% confidence and 19% coverage and 75% of the main Domain to be identical between homologues with and confidence of 100%. (Screenshots were obtained from the Phyre2 web portal, Kelley et al., 2015, [83])

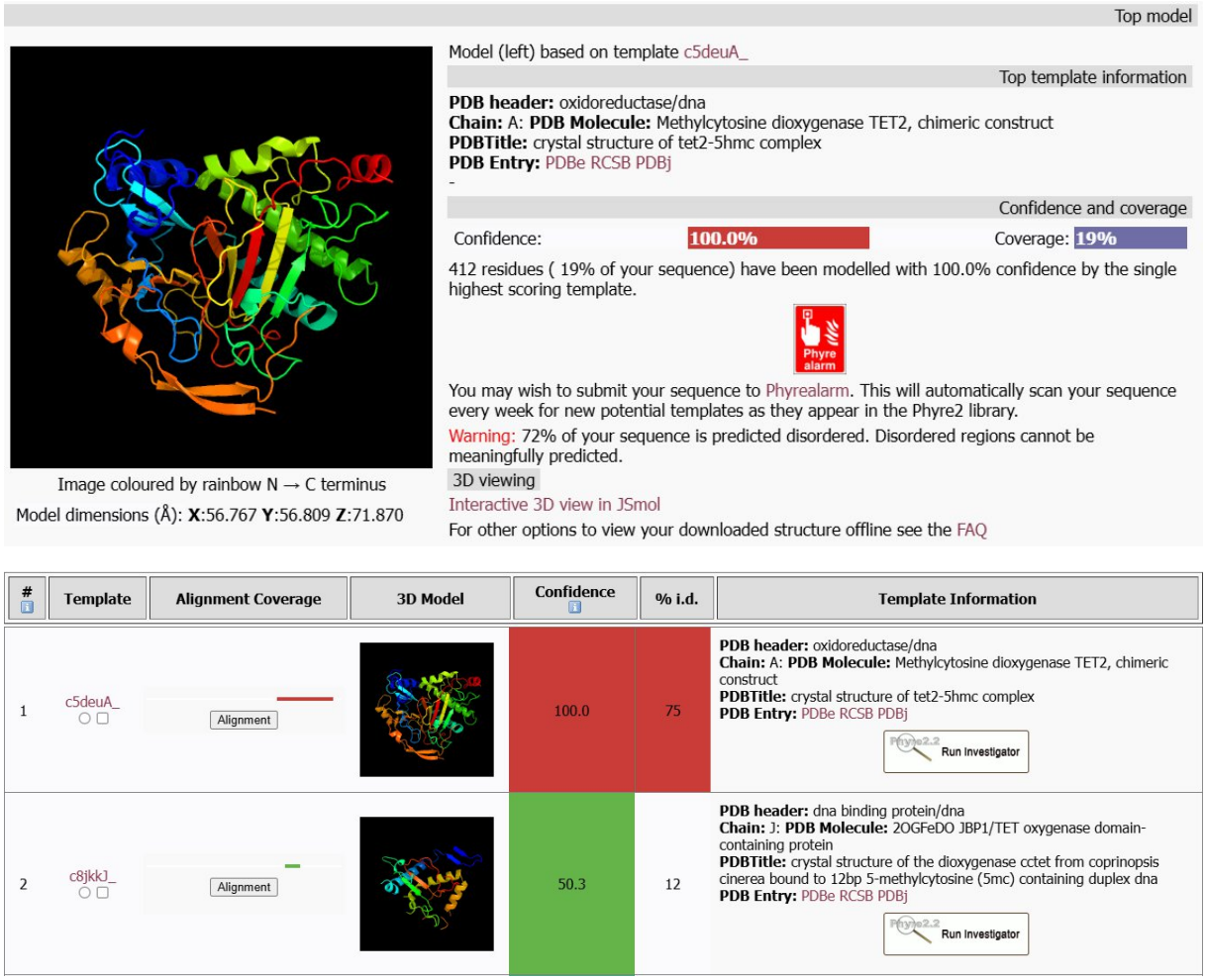

Supplementary Figure 4 Phyre2.2 homology modeling results for *N. furzeri* TET3 protein sequences. The analysis identified the crystal structure of human TET3 as the top template with 100% confidence and 19% coverage and 75% of the main Domain to be identical between homologues with and confidence of 100%. (Screenshots were obtained from the Phyre2 web portal, Kelley et al., 2015, [83]

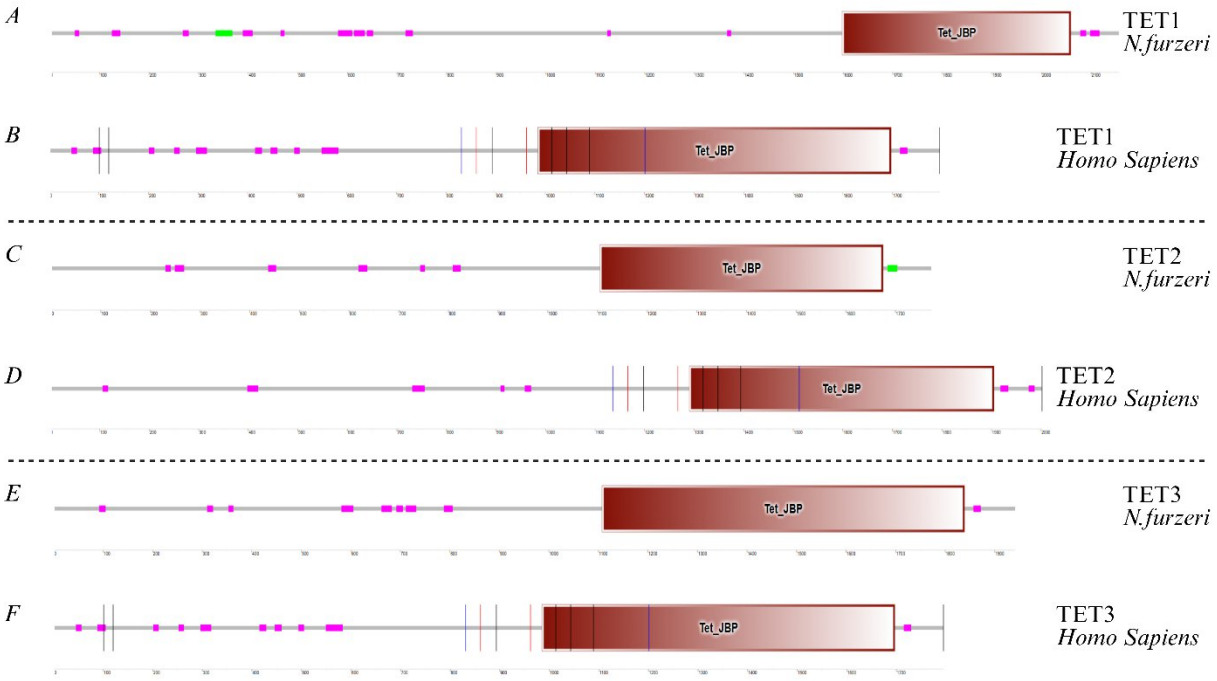

Supplementary Figure 5 Comparison of the TET enzyme family in *N. furzeri* and *Homo sapiens*, illustrating differences in protein size and domain positioning between species. (Screenshots were obtained from the SMART web portal, Letunic et al., 2020, [84])

9. Acknowledgements

First and foremost, I would like to thank Christoph Englert for giving me the opportunity to work on this project and for allowing me to grow and learn by facing scientific challenges. I am also grateful to Ulrich Technau for his continuous support throughout my master's studies and for his patient guidance during inevitable detours along the way.

My deepest gratitude goes to my supervisor, Hanna Mörl, who did an outstanding job not only in introducing me to the topic, but also in teaching me everything necessary to navigate the laboratory, the institute, and beyond. Her clear and structured guidance not only eased my path but also created a learning environment that was as supportive and healthy as one could wish for.

I also wish to thank the entire working group for creating such a pleasant and collaborative atmosphere. Special thanks go to Dagmar and Christina, who were always ready to help with technical issues. My sincere thanks as well to Annekatrin, Birgit, Caro, Nathalie, Abhishek**,** and Anastasija, who made my work easier and more enjoyable through their helpful advice and by contributing to the positive lab spirit. A very special thanks goes to Max Möscheid, whose immense knowledge, ideas, and suggestions - often shared during runs, cycles, or coffee breaks - were a constant source of inspiration and problem-solving, especially during the challenges of cloning procedures.

I am further thankful to the fish facility staff, whose careful work in mating the fish and collecting eggs was essential for my experiments, and to the FACS facility staff, who made an important contribution to planning and conduction of lentiviral experiments. In particular, I would like to thank Michael Müller for his kind and supportive assistance in this regard. As well a big thanks to Mara Sannai, who helped a lot sharing her knowledge about transfection using Lentiviral constructs.

Finally, I am deeply grateful to my family for their constant support and belief in me, and to my friends, especially Lydia and Aisha for uplifting me during the darker winter days when cloning attempts failed, lab work piled up, and the weather matched the mood.

Thank you all!

10. Declaration of authenticity

I hereby certify that I have written this thesis independently and that I have not used any sources or aids other than those indicated that all statements taken verbatim or in spirit from other writings have been identified, and that the thesis in the same or a similar version has not yet been part of a course of study or examination.

Brian Schild, Jena 01.10.2025